ACTIVE FIRES

VISIBLE/INFRARED IMAGER/RADIOMETER SUITE ALGORITHM THEORETICAL BASIS DOCUMENT

Version 4: May 2001

Shawn W. Miller
Quanhua Liu

RAYTHEON COMPANY
Information Technology and Scientific Services
4400 Forbes Boulevard
Lanham, MD 20706

SRBS Document #: Y3252

APPLICATION: ACTIVE FIRES

Doc No: Y3252

Version: 4

Revision: 0

	Function	Name	Signature	Date
Prepared by	Algorithm Developer	S. MILLER		
Approved by	Relevant IPT Lead	S. MILLER		
Reviewed by	Reviewer	K. JENSEN		
Approved by	Chief Scientist	S. MILLER		
Released by	Algorithm Lead	P. KEALY		

TABLE OF CONTENTS

Page

LIST OF FIGURES

LIST OF TABLES

GLOSSARY OF ACRONYMS

AOT	Aerosol Optical Thickness
ATB	Algorithm Theoretical Basis
ATBD	Algorithm Theoretical Basis Document
AVHRR	Advanced Very High Resolution Radiometer
BBR	Band-to-Band Registration
DoD	Department of Defense
EDR	Environmental Data Record
EOS	Earth Observing System
GIFOV	Ground Instantaneous Field of View
GOES	Geostationary Operational Environmental Satellite
GSD	Ground Sampling Distance
HCS	Horizontal Cell Size
HSR	Horizontal Spatial Resolution
HSS	Hazard Support System
IFOV	Instantaneous Field of View
IPO	Integrated Program Office
LQF	Land Quality Flag(s)
MODIS	Moderate Resolution Imaging Spectroradiometer
MODTRAN	Moderate Resolution Transmission Model
MTF	Modulation Transfer Function
NASA	National Aeronautics and Space Administration
NASA/GSFC	NASA Goddard Space Flight Center
NASA/JPL	NASA Jet Propulsion Laboratory
NDVI	Normalized Difference Vegetation Index
NIR	Near Infrared
NOAA	National Oceanic and Atmospheric Administration
NPOESS	National Polar-orbiting Operational Environmental Satellite System
NPP	NPOESS Preparatory Project
OLS	Operational Linescan System
PDR	Preliminary Design Review
PF	Potential Fire
RDR	Raw Data Record
SBRS	Santa Barbara Remote Sensing
SNR	Signal-to-Noise Ratio
SRD	Sensor Requirements Document
TIROS	Television Infrared Observation Satellite
TM	Thematic Mapper
TOA	Top of Atmosphere
VIIRS	Visible/Infrared Imager/Radiometer Suite

ABSTRACT

Active Fires is one of more than two dozen products explicitly required to be derived from the Visible/Infrared Imager/Radiometer Suite (VIIRS) sensor slated to fly onboard the National Polar-orbiting Operational Environmental Satellite System (NPOESS), which is scheduled for launch in 2008. The requirements for the VIIRS EDRs are described in detail in the VIIRS Sensor Requirements Document (SRD). These requirements form the foundation from which both the algorithms and the sensor are designed and built. A revised version of the SRD was released in November 1999, detailing a set of new requirements targeted toward the NPOESS Preparatory Project (NPP), a National Aeronautics and Space Administration (NASA) endeavor to build upon the MODIS heritage beginning in 2005. The Active Fires environmental data record (EDR) was added to the VIIRS SRD at that time. The most recent version of the VIIRS SRD remapped Active Fires to the status of an Application, under the heading of the Surface Type EDR. The Active Fires Application will consist of three distinct components: the detection of a fire or fires within a given geolocated VIIRS pixel; the subpixel average temperature of the fire or fires detected; and the subpixel area of the fire or fires detected. These latter two components represent a significant step forward in operational remote sensing of fires from space. This document includes a thorough description of the algorithm used to retrieved the product components listed above. Fire detection is based on contextual analysis; fire temperature and area retrieval are based on an extension of the two-band technique described in Dozier (1981). Additionally, Raytheon proposes to investigate the feasibility of adding a burn scar detection parameter to the product output as part of Phase II algorithm development. As Active Fires is a relatively new application for VIIRS, this document will not provide the level of detail, particularly concerning variance and performance estimates, that has been possible for the other VIIRS ATBDs. Such information will be provided in a later version of this document as it becomes available, and much of those data will originate with MODIS analyses and simulations.

1.0 INTRODUCTION

1.1 PURPOSE

This algorithm theoretical basis document (ATBD) describes the algorithms used to retrieve the Active Fires Application for the Visible/Infrared Imager/Radiometer Suite (VIIRS). Active Fires consists of three distinct components: detection of fires; subpixel average temperature of detected fires; and subpixel area of detected fires. This document will describe the required inputs, a theoretical description of the algorithms, the sources and magnitudes of the errors involved, practical considerations for post-launch implementation, and the assumptions and limitations associated with the products. Table 1 summarizes the three components of the Active Fires Application. SRD is an acronym for the VIIRS Sensor Requirements Document (IPO, 2000).

Table 1. Component products of the Active Fires Application.

Component	Description	Purpose
Fire Detection	Flagging of a given geolocated VIIRS pixel to indicate the presence of an active fire or fires within, which is assigned to the center latitude and longitude of the pixel.	Operational monitoring of fires, launching point for evaluation of more detailed parameters which serve both operational and research purposes.
Subpixel Average Fire Temperature (SAFT)	The average temperature of all surfaces within a fire-detected pixel that are overlain by an active fire or fires.	Feeds into tactical issues for handling of fires, aids the computation of energy/aerosol/carbon fluxes into the atmosphere
Subpixel Fire Area (SFA)	The projection of the total area of all surfaces within a fire-detected pixel that are overlain by an active fire or fires onto a plane perpendicular to the normal vector at the center of the pixel.	Feeds into tactical issues for handling of fires, aids the computation of energy/aerosol/carbon fluxes into the atmosphere

1.2 SCOPE

This document covers the algorithm theoretical basis (ATB) for the operational retrieval of the Active Fires Application. Any derived products beyond the three components of Active Fires will not be discussed beyond brief mention. The exact structure of the algorithms for the Active Fires EDR may change during the developmental phase of this experiment; this document will be revised accordingly to match those changes. Only the algorithms that will be implemented for routine operational processing will be preserved in the final release of this document.

Section 1 describes the purpose and scope of this document; it also includes a listing of VIIRS documents that will be cited in the following sections. Section 2 provides a brief overview of the motivation for the Active Fires algorithm, including the objectives of the retrievals, the currently designed VIIRS instrument characteristics, and the strategy for retrieval of the Active Fires product. Section 3 contains the essence of this document—a complete description of the Active Fires Application and its components. Consideration is given to the overall structure, the required inputs, a theoretical description of the algorithm, assessment of the error budget, results of ongoing sensitivity studies, practical implementation issues, and recommendations for product validation. Section 4 provides an overview of the constraints, assumptions and limitations associated with the Active Fires EDR, and Section 5 contains a listing of non-VIIRS references cited throughout the course of this document.

1.3 VIIRS DOCUMENTS

Reference to VIIRS documents within this ATBD will be indicated by an italicized Raytheon Santa Barbara Remote Sensing (SBRS) official Y-number in brackets, e.g., *[Y2388]*.

Y2388 VIIRS Aerosol Optical Thickness and Aerosol Particle Size Parameter ATBD

Y2390 VIIRS Suspended Matter ATBD

Y2393 VIIRS Cloud Effective Particle Size and Cloud Optical Thickness ATBD

Y2400 VIIRS Vegetation Index ATBD

Y2402 VIIRS Surface Type ATBD

Y2411 VIIRS Surface Reflectance ATBD

Y2412 VIIRS Cloud Mask ATBD

Y2468 VIIRS Operations Concept Document

Y2469 VIIRS Context Level Software Architecture

Y2470 VIIRS Interface Control Document (ICD)

Y2474 VIIRS Land Module Level Software Architecture

Y2483 VIIRS Land Module Level Detailed Design

Y3236 VIIRS Software Integration and Test Plan

Y3237 VIIRS Algorithm Verification and Validation Plan

Y3251 VIIRS Precipitable Water ATBD

Y3257 VIIRS Computer Resources Requirements Document

Y3261 VIIRS Radiometric Calibration ATBD

Y3270 VIIRS System Verification and Validation Plan

Y3279 VIIRS Land Module Level Interface Control Document

Y3283 VIIRS Active Fires Unit Level Detailed Design

Y6635 VIIRS Algorithm Software Development Plan

Y6661 VIIRS Algorithm Software Maturity Assessment

Y7040 VIIRS Algorithm/Data Processing Technical Report

Y7051 VIIRS Earth Gridding ATBD

SS154650 VIIRS System Specification

PS154650 VIIRS Sensor Specification

PS154640 VIIRS Algorithm Specification

1.4 REVISION HISTORY

This is the second working version of this document, however it is labeled Version 4 to match it with the delivery of the other VIIRS ATBDs. It is dated May 2001. The first working version, Version 3, was dated May 2000. The authors would like to thank Luke Flynn for a number of insightful discussions in Phase I algorithm development, and Eric Vermote and Louis Giglio for further guidance in Phase II. This document has been significantly revised since Version 3. The primary areas in which changes have been made are:

1) Detail now given on the logical and mathematical structure of the detection and temperature/area measurement algorithms

2) Updated VIIRS band names and associated saturation characteristics

3) Updated status of saturation handling strategy, including new details on the use of the shortwave infrared (SWIR) bands

2.0 EXPERIMENT OVERVIEW

2.1 OBJECTIVES OF ACTIVE FIRES RETRIEVALS

As pointed out in the MODIS Fire Products ATBD (Kaufman and Justice, 1998), fire is an important process in many terrestrial biomes, and the release of gases and particulate matter during biomass burning is an important contributor to the chemical reactions and physical processes taking place in the atmosphere. Fire is a significant factor in the ecology of savannas, boreal forests, and tundra, and it plays a central role in deforestation in tropical and sub-tropical regions.

Severe fires have large impacts on climate changes. Fires change the physical state of the vegetation, releasing a variety of greenhouse gases into the atmosphere. There is presently great uncertainty as to the magnitude of the sources and sinks of these greenhouse gases. The release of chemically reactive gases during biomass burning strongly influences chemical processes within the troposphere. It is estimated that annual biomass burning may be associated with 38% of the ozone in the troposphere; 32% of global carbon monoxide; more than 20% of the world's hydrogen, non-methane hydrocarbons, methyl chloride and oxides of nitrogen; and approximately 39% of the particulate organic carbon (Levine, 1991; Andreae, 1991; Kaufman *et al*., 1998a,b).

Satellite data have been widely applied to the monitoring of fires over vegetated land, especially over forests. The Advanced Very High Resolution Radiometer (AVHRR), Geostationary Operational Environmental Satellite (GOES), and Geostationary Meteorological Satellite (GMS) have all been successfully utilized for monitoring severe fires in California, Brazil, China, and Indonesia. The remote sensing of fire aftermaths has also received considerable attention, as fires have a propensity for making abrupt, large-scale changes in the vegetation index (see Figure 1).

Figure 1. Forest fire altering the landscape (from www.cnn.com).

The global distribution of active vegetation fires can be derived from AVHRR data, as seen in Figure 2. The area of an active fire can be smaller than a square meter or larger than 100 square kilometers.

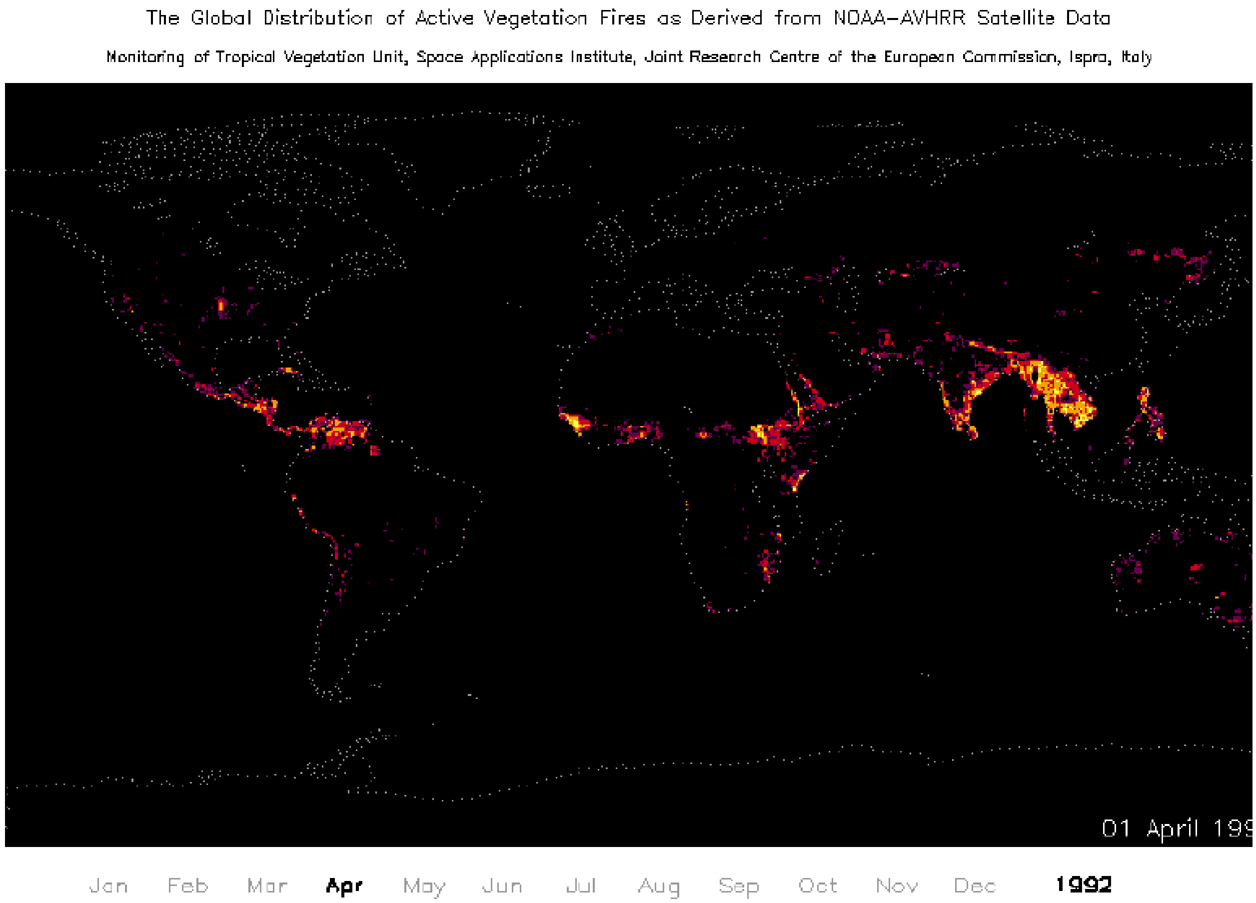

Figure 2. The global distribution of active vegetation fires as derived from NOAA-AVHRR satellite data for April 1, 1999 (from NOAA web site).

Figure 3 shows the capabilities of GOES for fire detection. Active fires are highlighted based on data from the midwave infrared (MWIR) band at 3.9 µm. Smoke from the fires can be seen from the visible band. Somewhat ironically of course, fire temperature and area measurement cannot be conducted where the fire is obscured by smoke, however active fires are almost always fed in part by strong winds, and these winds tend to blow smoke plumes clear of the majority of the burning area, as seen in Figure 3.

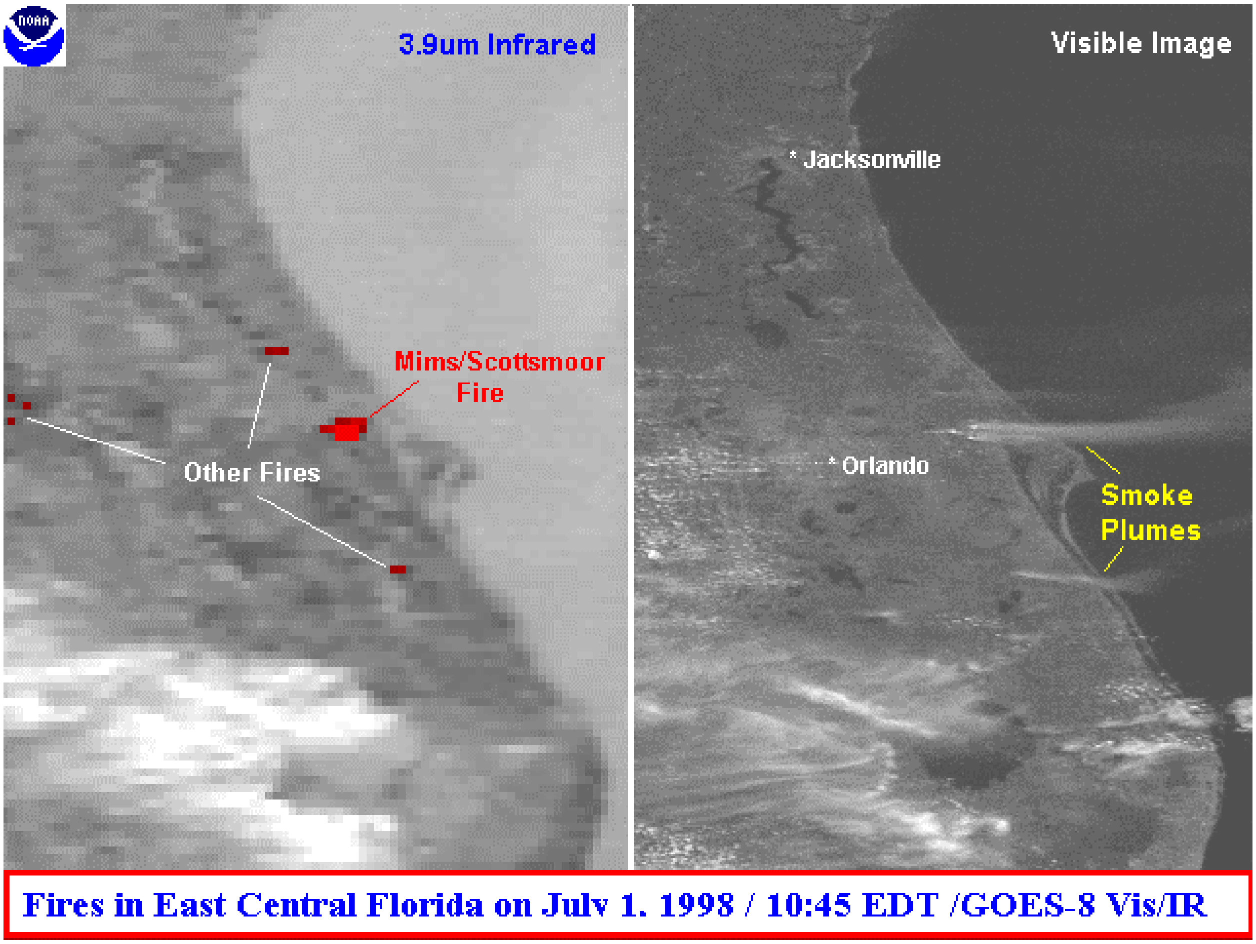

Figure 3. GOES-8 visible/IR image used to detect fires (red indicates active fires). From NOAA web site.

2.2 INSTRUMENT CHARACTERISTICS

The VIIRS instrument will now be briefly described to clarify the context of the descriptions of the Active Fires Application presented in this document. VIIRS can be pictured as a convergence of three existing sensors, two of which have seen extensive operational use at this writing.

The Operational Linescan System (OLS) is the operational visible/infrared scanner for the Department of Defense (DoD). Its unique strengths are controlled growth in spatial resolution through rotation of the ground instantaneous field of view (GIFOV) and the existence of a low-level light sensor (LLLS) capable of detecting visible radiation at night. OLS has primarily served as a data source for manual analysis of imagery. The Advanced Very High Resolution Radiometer (AVHRR) is the operational visible/infrared sensor flown on the National Oceanic and Atmospheric Administration (NOAA) Television Infrared Observation Satellite (TIROS-N) series of satellites (Planet, 1988). Its unique strengths are low operational and production cost and the presence of five spectral channels that can be used in a wide number of combinations to produce operational and research products. In December 1999, the National Aeronautics and Space Administration (NASA) launched the Earth Observing System (EOS) morning satellite, *Terra*, which includes the Moderate Resolution Imaging Spectroradiometer (MODIS). This sensor possesses an unprecedented array of thirty-two spectral bands at resolutions ranging from 250 m to 1 km at nadir, allowing for currently unparalleled accuracy in a wide range of satellite-based environmental measurements.

VIIRS will reside on a platform of the National Polar-orbiting Operational Environmental Satellite System (NPOESS) series of satellites. It is intended to be the product of a convergence between DoD, NOAA and NASA in the form of a single visible/infrared sensor capable of satisfying the needs of all three communities, as well as the research community beyond. As such, VIIRS will require three key attributes: high spatial resolution with controlled growth off nadir, minimal production and operational cost, and a large number of spectral bands to satisfy the requirements for generating accurate operational and scientific products.

Figure 4 illustrates the design concept for VIIRS, designed and built by Raytheon Santa Barbara Remote Sensing (SBRS). At its heart is a rotating telescope scanning mechanism that minimizes the effects of solar impingement and scattered light. Calibration is performed onboard using a solar diffuser for short wavelengths and a V-groove blackbody source and deep space view for thermal wavelengths. A solar diffuser stability monitor (SDSM) is also included to track the performance of the solar diffuser. The nominal altitude for NPOESS will be 833 km. The VIIRS scan will extend to 56 degrees on either side of nadir.

The VIIRS SRD places explicit requirements on spatial resolution for the Imagery EDR. Specifically, the horizontal spatial resolution (HSR) of bands used to meet threshold Imagery EDR requirements must be no greater than 400 m at nadir and 800 m at the edge of the scan. This led to the development of a unique scanning approach which optimizes both spatial resolution and signal to noise ratio (SNR) across the scan. The concept is summarized in Figure 5 for the imagery bands; the nested lower resolution radiometric bands follow the same paradigm at exactly twice the size. The VIIRS detectors are rectangular, with the smaller dimension projecting along the scan. At nadir, three detector footprints are aggregated to form a single VIIRS "pixel." Moving along the scan away from nadir, the detector footprints become larger both along track and along scan, due to geometric effects and the curvature of the Earth. The effects are much larger along scan. At around 32 degrees in scan angle, the aggregation scheme is changed from 3x1 to 2x1. A similar switch from 2x1 to 1x1 aggregation occurs at 48 degrees. The VIIRS scan consequently exhibits a pixel growth factor of only 2 both along track and along scan, compared with a growth factor of 6 along scan which would be realized without the use of the aggregation scheme. Figure 6 illustrates the benefits of the aggregation scheme for spatial resolution.

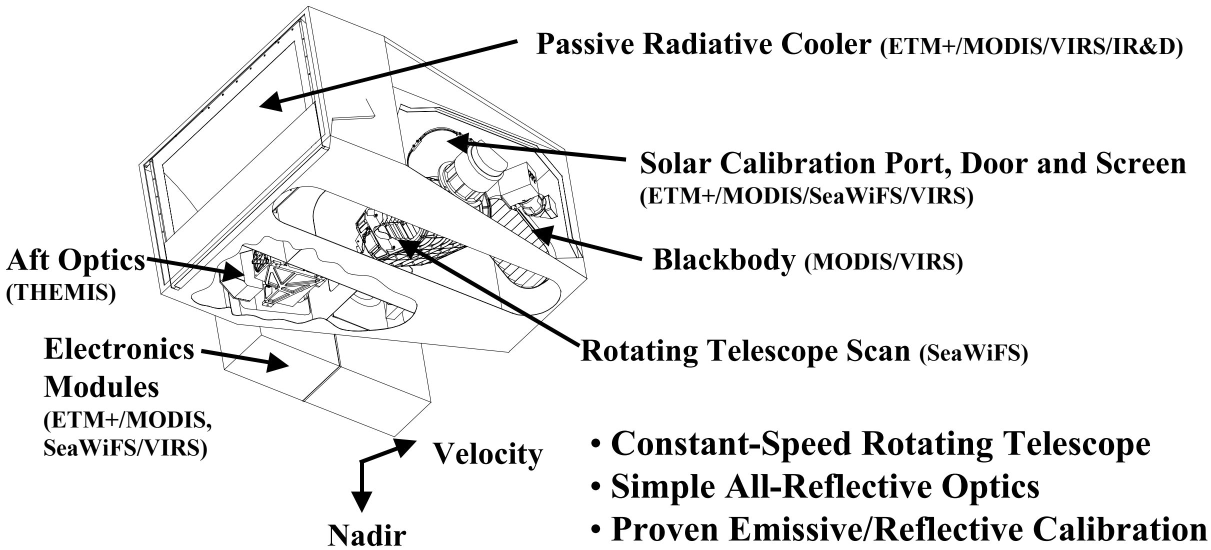

Figure 4. Summary of VIIRS design concepts and heritage.

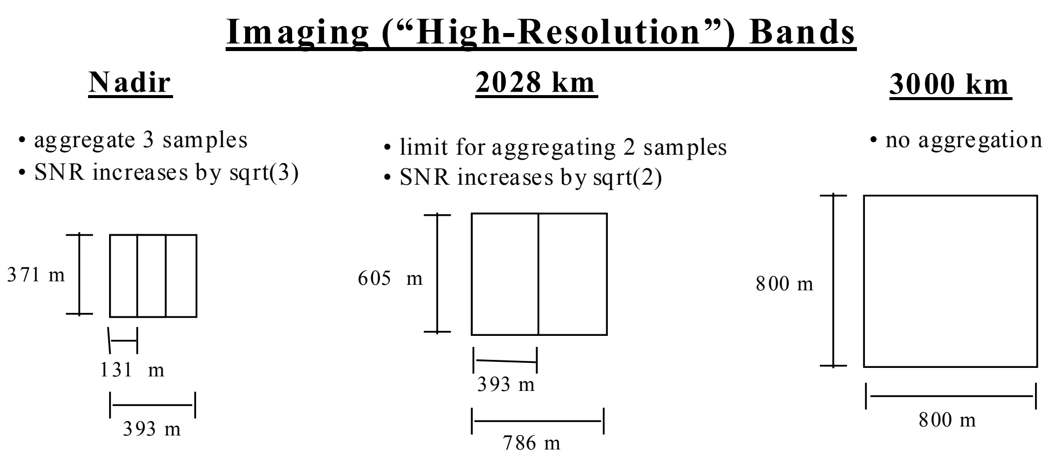

Figure 5. VIIRS detector footprint aggregation scheme for building "pixels."

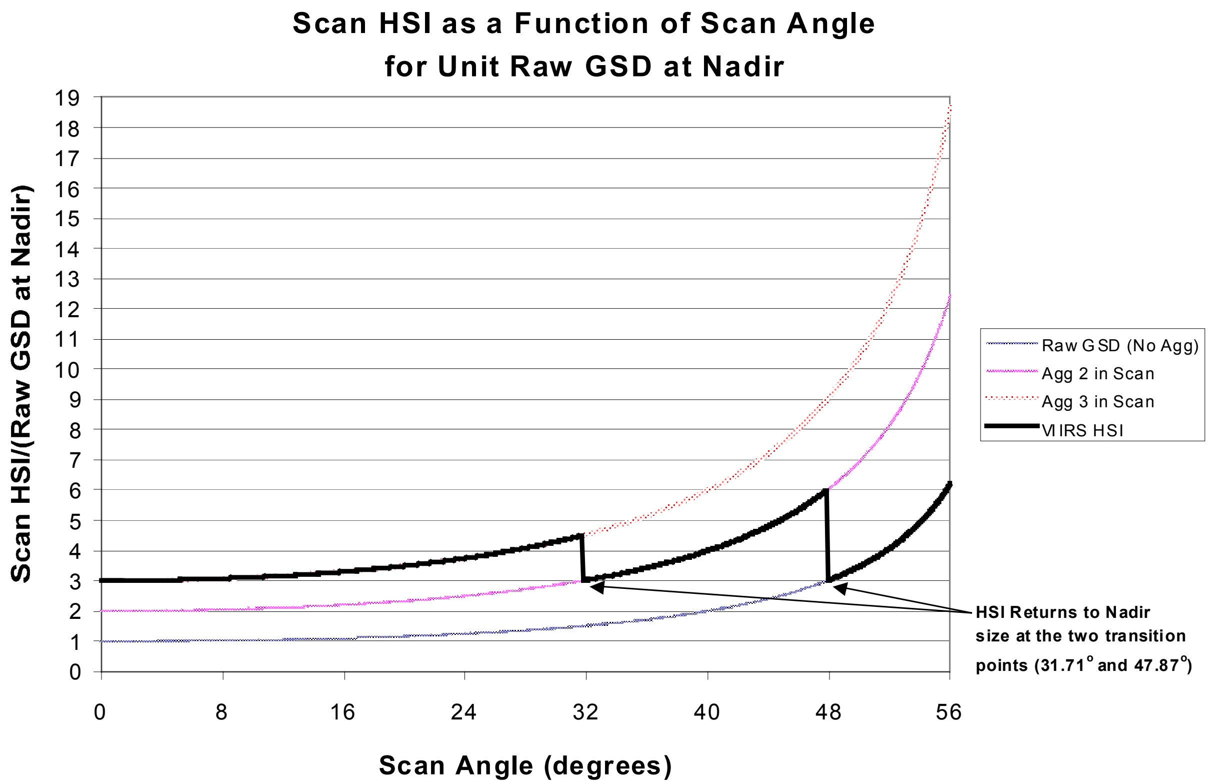

Figure 6. Benefits of VIIRS aggregation scheme in reducing pixel growth at edge of scan.

This scanning approach is extremely beneficial for the retrieval of land products such as Active Fires, although the improved spatial resolution at the edge of the swath also increases the chances of band saturation compared to other instruments such as MODIS.

The positioning of the VIIRS spectral bands is summarized in Figure 7 through Figure 10. Table 2 summarizes the saturation characteristics of the instrument in the bands relevant to Active Fires. "Tmax" is the saturation temperature in the band. "Lbmax" is band radiance in $Wcm^{-2}sr^{-1}$. "Lmax" is spectral radiance in $W\ m^{-2}sr^{-1}\mu m^{-1}$. "Rmax" is reflectance. The issue of saturation will be addressed again in Section 3.3.2.3, as it has had a significant impact on the strategy for Active Fires algorithm development. A detailed summary of the radiometric, spatial, and spectral characteristics of VIIRS can be found in the VIIRS Sensor Specification *[PS154650]*.

Table 2. VIIRS band saturation characteristics relevant to Active Fires.

Band	Center	Width	Solar	Tmax	Lbmax	Lmax	Rmax
M7	0.8650	0.0390	310.2	**1215**	1.09E-03	278.78	0.899
M8	1.2400	0.0200	149.2	**895**	1.90E-04	95.14	0.638
M10	1.6100	0.0600	78.1	**749**	4.35E-04	72.45	0.928
M11	2.2500	0.0500	24	**577**	1.59E-04	31.76	1.323
M13	4.0500	0.1550	---	**634**	6.27E-03	404.27	---
M15	10.7625	1.0000	---	**343**	1.71E-03	17.08	---
I5	11.4500	1.9000	---	**340**	2.93E-03	15.41	---

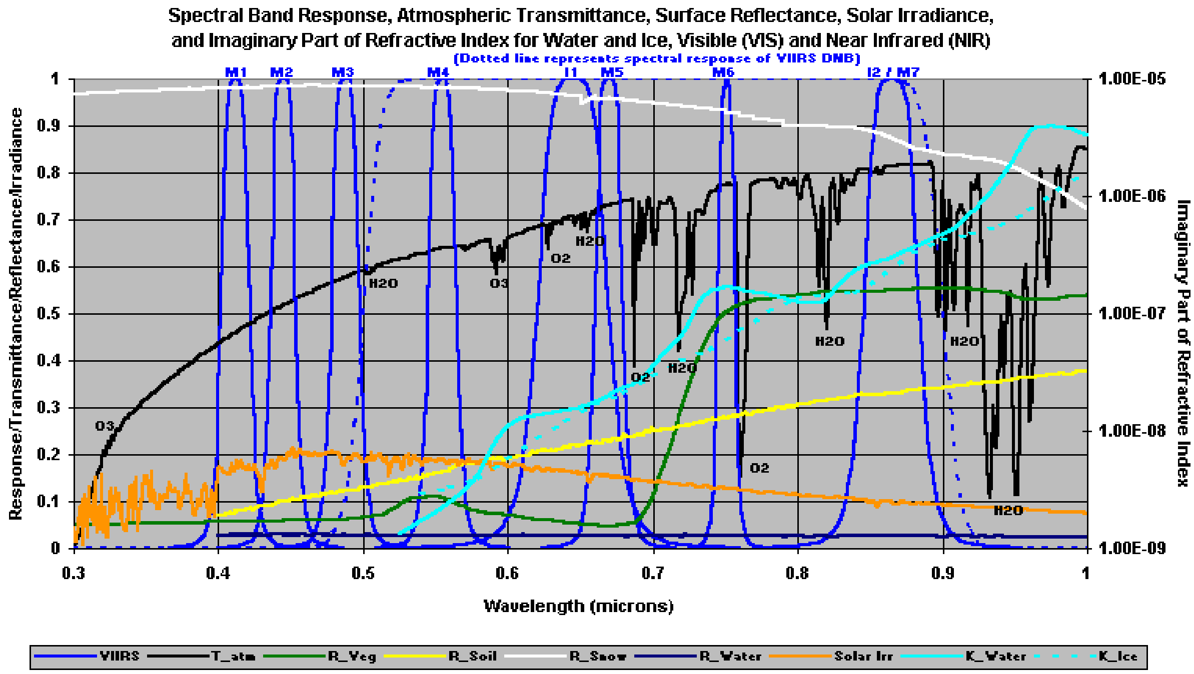

Figure 7. VIIRS spectral bands, visible and near infrared (VNIR).

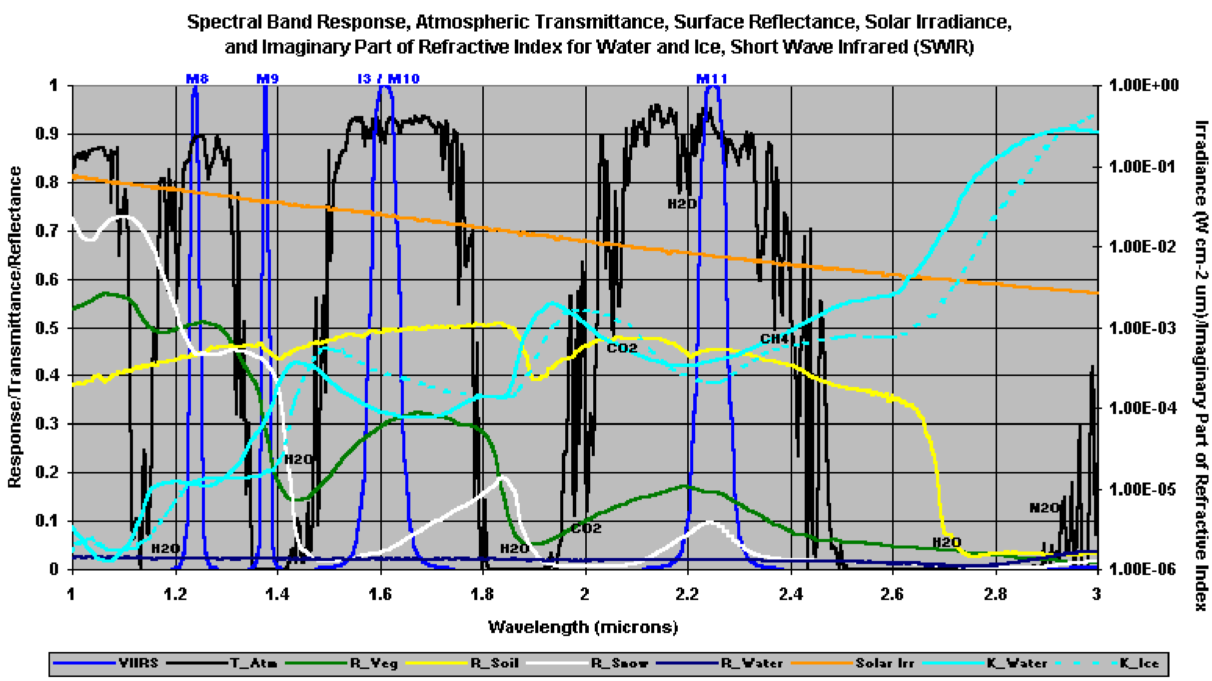

Figure 8. VIIRS spectral bands, shortwave infrared (SWIR).

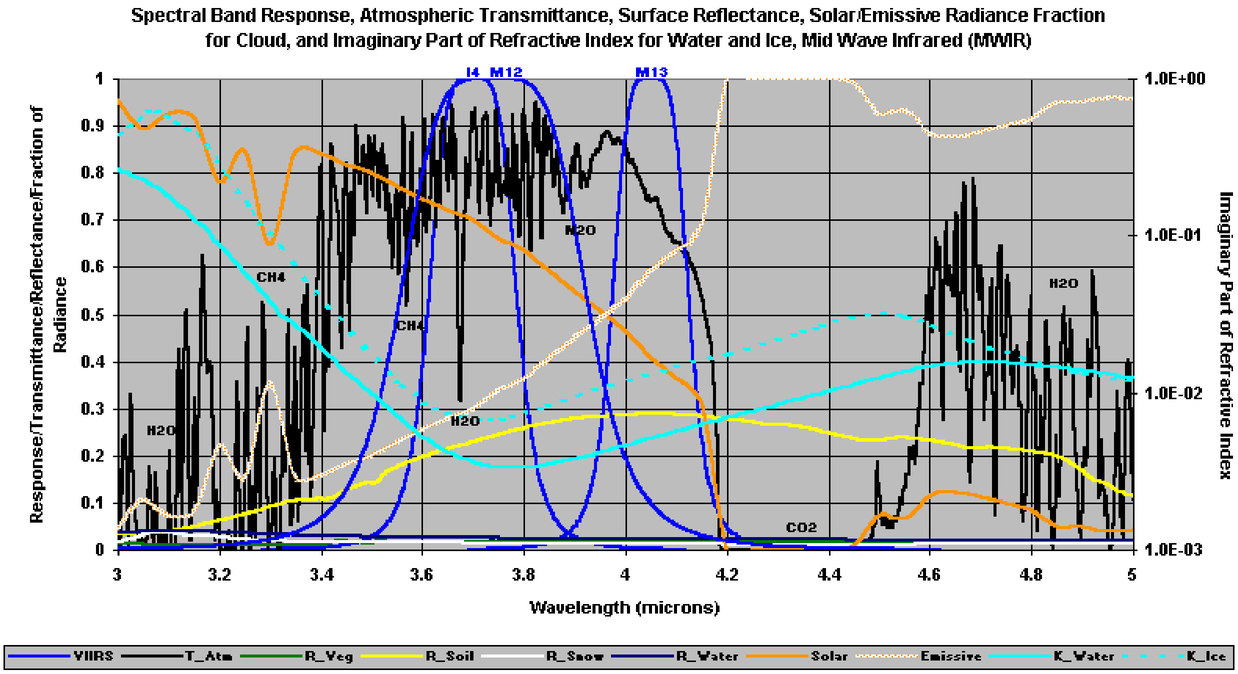

Figure 9. VIIRS spectral bands, midwave infrared (MWIR).

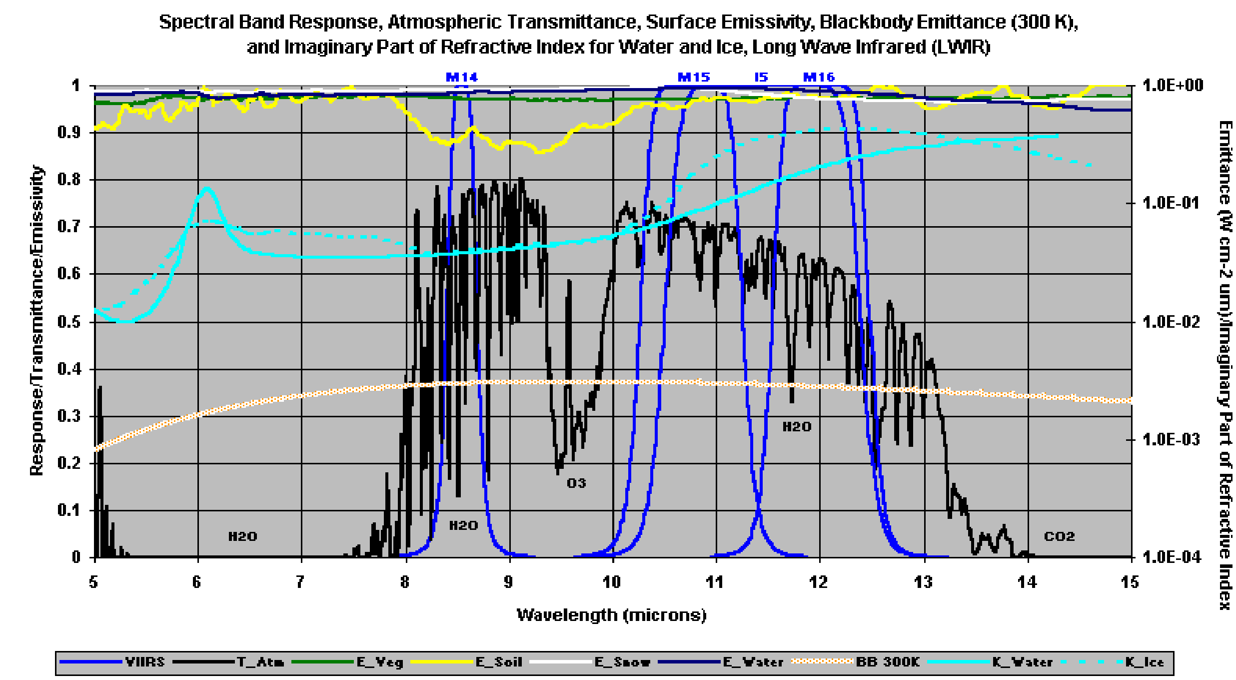

Figure 10. VIIRS spectral bands, longwave infrared (LWIR).

2.3 RETRIEVAL STRATEGY

The Active Fires product is retrieved over land, both day and night, under clear conditions. Land is defined as anything not categorized as ocean by the land/sea mask present in the VIIRS Cloud Mask output. Day is defined by a solar zenith angle of 85 degrees or less. The only difference between day and night processing is that the solar signal must be removed from the reflective bands prior to implementation of the Active Fires algorithm. This removal will take place within the Active Fires unit level code. “Clear” means that the pixel in question is classified by the VIIRS Cloud Mask as either “clear,” “probably clear,” or "probably cloudy." If the pixel is classified as "probably clear" or "probably cloudy," the VIIRS Land Quality Flag (LQF) output, appended to the Surface Reflectance IP *[Y2411]*, will include a flag indicating possible cloud contamination. The VIIRS SRD requires Active Fires to be retrieved under conditions of “broken clouds,” however this is interpreted to mean that the pixel in question may be surrounded by cloudy pixels, yet itself is classified as “confident clear,” “probably clear,” or "probably cloudy."

The VIIRS operations concept stipulates that four nominally reflectance-based bands—M7 (865 nm), M8 (1.24 µm), M10 (1.61 µm), and M11 (2.25 µm)—will be active both day and night to facilitate the retrieval of the Active Fires product. These bands are crucial for the measurement of fire temperature and area in instances of large and/or very hot fires, since the LWIR bands saturate in such conditions. Table 3 summarizes the bands used for retrieval of the Active Fires Application. Imagery resolution bands are presently being considered solely for detection purposes, but the baseline algorithm relies on moderate resolution bands alone. Moderate resolution bands are used for both detection and the measurement of fire temperature and area. The hotter and/or larger the fire, the shorter the wavelengths necessary to retrieve its temperature and area. Retrieval of fires during the 1730 (terminator) orbit will be of great use, as this is the time during which fires typically reach their peak, after a day’s worth of solar heating.

Table 3. VIIRS bands used for Active Fires Application.

Band	Center Wavelength (µm)	Nadir resolution (m)	Usage for Active Fires
M8	1.24	750	Temperature/area measurement for very hot/large fires
M10	1.61	750	Temperature/area measurement for very hot/large fires
M11	2.25	750	Temperature/area measurement for very hot/large fires
I4	3.74	375	Detection (research level consideration)
M13	4.05	750	Detection/temperature/area measurement
M15	10.76	750	Detection/temperature/area measurement
I5	11.45	375	Detection (research level consideration)

3.0 ALGORITHM DESCRIPTION

3.1 PROCESSING OUTLINE

Figure 11 illustrates the general processing architecture for the Active Fires Application. The moderate resolution brightness temperatures in bands M13 (4.05 µm) and M15 (10.76 µm) are used for detection, and the moderate resolution brightness temperatures in bands M7 (865 nm), M8 (1.24 µm), M10 (1.61 µm), M11 (2.25 µm), M13, and M15 are targeted toward the subsequent fire/area calculations. The Surface Type *[Y2402]* and Vegetation Index *[Y2400]* EDRs will aid in characterization of the background, and the Cloud Mask Intermediate Product (IP, *[Y2412]*) includes sunglint detection to prevent false alarms over inland water bodies. More detail on the box labeled "Calculation of Fire Temperature and Area," including the handling of band saturation, is provided in Sections 3.3.2.2 and 3.3.2.3.

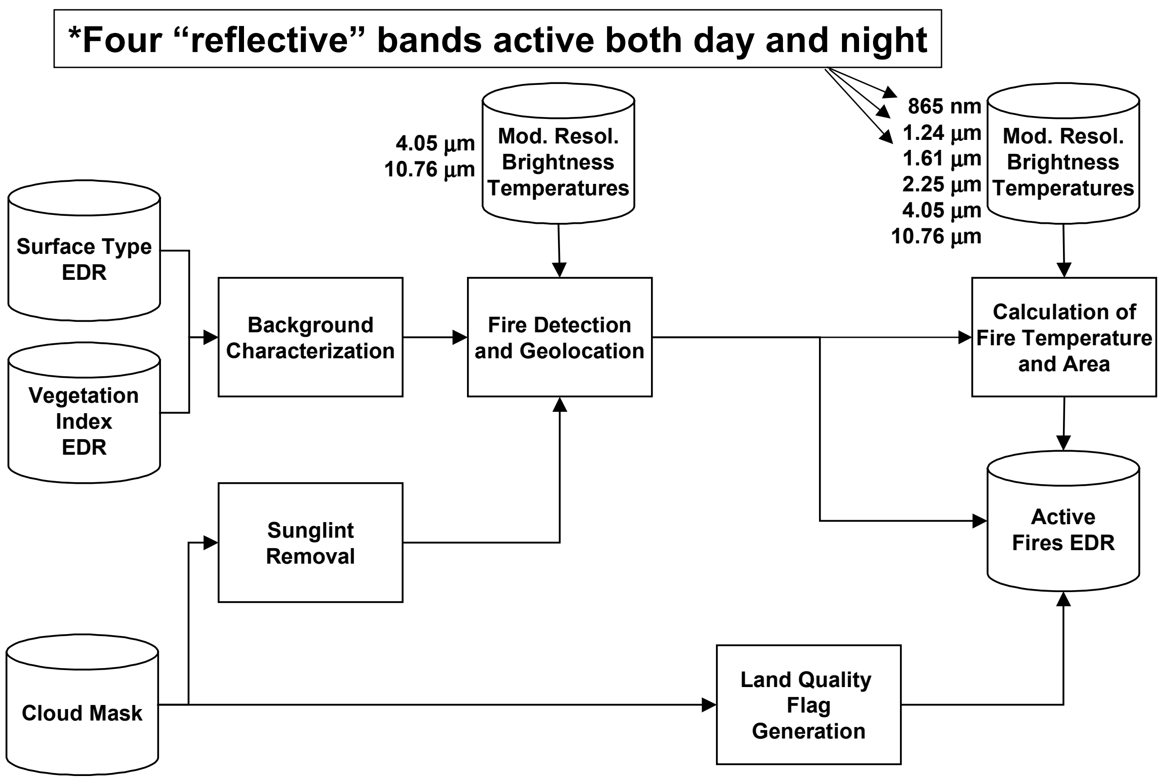

Figure 11. Processing architecture for Active Fires Application.

3.2 ALGORITHM INPUT

3.2.1 VIIRS Data

The Active Fires product requires as input, at a minimum, the Calibrated TOA Brightness Temperatures Sensor Data Record (SDR). This data flow includes both calibrated brightness temperatures in the necessary bands and the required accompanying information, including solar/viewing geometry and geolocation information. The Vegetation Index and Surface Type

EDRs provide additional information that reduces errors in the characterization of the background. The Cloud Mask IP output includes a sunglint flag.

Four additional types of inputs from VIIRS are expected to be required, but the handling of these inputs has not yet been developed, and they are not shown in Figure 11. These inputs provide information about surface properties, aerosols, clouds, and precipitable water that are very important for correction of fire temperature and area calculations.

The Gridded Weekly Surface Reflectance (GWSR) IP will be required during the day, i.e., for a solar zenith angle of 85 degrees or less. This product is already being generated for the purposes of the Cloud Optical Properties EDRs. The algorithm for producing the GWSR IP is summarized in the VIIRS Earth Gridding ATBD *[Y7051]*. When band M15 saturates, it will be necessary to move into the shortwave infrared (SWIR) and possibly the near infrared (NIR) to assist in the retrieval of fire temperature and area. During the daytime, the SWIR and NIR bands are, in this context, contaminated by a solar reflective signal that depends on the surface type, solar/viewing geometry, and atmospheric conditions. The GWSR IP, together with the solar/viewing geometry for the pixel in question, may allow for algorithmic removal of this reflective signal so that the emissive signal from the fire can be isolated for fire temperature/area calculations.

The VIIRS Aerosol Optical Thickness *[Y2388]* and Suspended Matter *[Y2390]* EDRs will be required as input to Active Fires processing, so that the effects of aerosols can be accounted for in the retrieval of surface brightness temperatures. To first order, the aerosols will tend to scatter the NIR and SWIR radiation and absorb in the MWIR and LWIR.

The VIIRS Cloud Effective Particle Size and Cloud Optical Thickness EDRs *[Y2393]* may be required as input if correctable thin cirrus is present, however the calculation of these quantities may be in question where fires exist. This issue will be discussed in more detail in Version 5 of this ATBD.

Finally, the Active Fires Application will require knowledge of the atmospheric water vapor present along the path between the surface and the sensor. VIIRS will be producing an EDR that supplies this information *[Y3251]*, however this EDR uses the MWIR and LWIR bands to retrieve precipitable water, and if a fire is present, the output water vapor estimation will be unreliable. Consequently, the baseline approach is to incorporate National Centers for Environmental Prediction (NCEP) analyses for column water vapor.

3.2.2 Non-VIIRS Data

As mentioned above, the only non-VIIRS input expected to be required for Active Fires processing is NCEP column water vapor.

3.3 THEORETICAL DESCRIPTION OF ACTIVE FIRES RETRIEVALS

3.3.1 Physics of the Problem

The physics underlying the retrieval of active fires is based on the enhanced thermal radiation caused by the high temperatures associated with smoldering and flaming fires. The peak of the surface emitted radiance shifts to shorter wavelengths as the surface temperature increases. The following sections detail the spectral and mathematical bases for fire retrievals.

3.3.1.1 Spectral Characteristics of Fires

Figure 12 illustrates the radiances typical of various types of fire/volcano scenarios at the Earth's surface, for nighttime conditions. The blackbody for a typical land surface temperature follows the traditional trend of increasing radiance into the longwave infrared (LWIR). A cooling lava flow is the next most similar curve, but its peak is well toward the midwave infrared (MWIR). A very active fire covering a very small portion of the pixel will exhibit a peak around 5 µm, and a larger active fire with a surrounding smoldering region extending throughout the pixel will push the peak of the blackbody curve down to 3 µm. The flaming portion of a fire can get as hot as 1800 K, at which point the blackbody curve shifts into the shortwave infrared (SWIR).

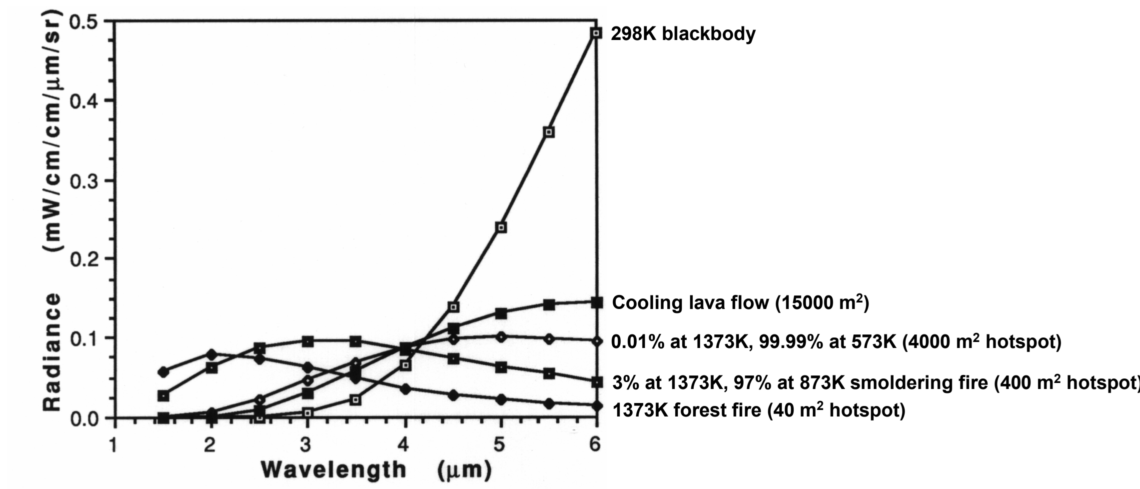

Figure 12. Radiance characteristics of fires in the midwave infrared (MWIR) portion of the spectrum, for nighttime conditions.

The sensitivity to active fires at 4.05 and 10.76 µm is different because of the different atmospheric absorption properties and the different behavior of the Planck function at the two wavelengths. As a fire becomes hotter or larger, its contribution to the total pixel radiance grows, and by Wein's displacement law it shifts into the shorter wavelengths. There are two general states of an active fire: flaming and smoldering. Flaming tends to occur around an average temperature of 1000 K, while smoldering tends to occur at a temperature of 600 K. These are merely averaged values, but they are suitable for the discussion at hand. Using these typical temperatures, one can calculate in the VIIRS bands what the maximum measurable area of smoldering or flaming fire would be for a given pixel. Table 4 through Table 9 on the following several pages summarize the capabilities of the relevant VIIRS bands heading into Phase II. Each table reports the brightness temperature in a given band corresponding to the fire temperature along the left and the fire area across the top. Brightness temperatures in red indicate the band has saturated. The two outermost shaded columns in each table signify roughly where the temperature/area measurement range resides when translated into VIIRS pixels at nadir (ignoring 3x1 aggregation for the present). The two right-most shaded columns give a better sense of what fraction of the area measurement range is met without saturation by a given band.

The shorter wavelength bands are undergoing adjustments to the specified maximum radiance; the results will be updated in Version 5 of this ATBD (saturation temperatures are only expected to increase after this activity).

Table 4. Pixel brightness temperatures and band saturation characteristics for VIIRS band M7 (865 nm).

865 nm	A (pixel)																					
T (K)	0	1E-09	1E-08	0.0000001	0.000001	0.00001	0.0001	0.001	0.005	0.01	0.02	0.03	0.04	0.05	0.06	0.067385	0.07	0.08	0.09	0.1	0.125	0.15
800	300	401	424	451	481	515	554	600	638	655	673	685	693	699	705	708	709	713	717	720	727	733
810	300	403	427	454	484	519	559	606	644	662	680	692	700	707	712	716	717	721	725	728	736	741
820	300	406	430	457	488	523	564	612	650	668	687	699	708	714	720	724	725	729	733	736	744	750
830	300	408	432	460	491	527	569	617	656	675	694	706	715	722	728	732	733	737	741	744	752	758
840	300	410	435	463	495	531	573	623	663	682	701	714	723	730	736	739	741	745	749	752	760	767
850	300	413	438	466	498	535	578	628	669	688	708	721	730	737	743	747	748	753	757	761	768	775
860	300	415	440	469	502	539	583	634	675	695	715	728	737	745	751	755	756	761	765	769	777	783
870	300	417	443	472	505	543	587	639	681	701	722	735	745	752	758	762	764	768	773	776	785	791
880	300	420	446	475	508	547	592	644	687	708	729	742	752	760	766	770	771	776	781	784	793	800
890	300	422	448	478	512	551	596	650	693	714	736	749	759	767	774	778	779	784	788	792	801	808
900	300	424	451	481	515	555	601	655	699	720	743	756	767	774	781	785	787	792	796	800	809	816
910	300	426	453	484	518	558	605	660	706	727	750	764	774	782	789	793	794	800	804	808	817	824
920	300	429	456	486	522	562	610	666	711	733	756	771	781	789	796	801	802	807	812	816	825	833
930	300	431	458	489	525	566	614	671	717	740	763	778	788	797	804	808	810	815	820	824	833	841
940	300	433	461	492	528	569	618	676	723	746	770	785	795	804	811	816	817	823	827	832	841	849
950	300	435	463	495	531	573	623	681	729	752	777	791	802	811	818	823	825	830	835	840	849	857
960	300	437	465	497	534	577	627	686	735	758	783	798	810	818	826	831	832	838	843	847	857	865
970	300	439	468	500	537	580	631	691	741	765	790	805	817	826	833	838	840	845	851	855	865	873
980	300	441	470	503	540	584	635	697	747	771	796	812	824	833	841	846	847	853	858	863	873	881
990	300	443	472	505	543	587	639	702	753	777	803	819	831	840	848	853	855	861	866	871	881	890
1000	300	445	475	508	546	591	644	707	758	783	810	826	838	847	855	860	862	868	874	878	889	898
1010	300	447	477	510	549	594	648	712	764	789	816	833	845	855	863	868	870	876	881	886	897	906
1020	300	449	479	513	552	598	652	716	770	795	823	839	852	862	870	875	877	883	889	894	905	914
1030	300	451	481	515	555	601	656	721	776	801	829	846	859	869	877	883	884	891	896	901	913	922
1040	300	453	483	518	558	605	660	726	781	807	836	853	866	876	884	890	892	898	904	909	920	930
1050	300	455	485	520	561	608	664	731	787	814	842	860	873	883	892	897	899	906	911	917	928	938
1060	300	457	488	523	564	611	668	736	792	819	848	866	880	890	899	905	906	913	919	924	936	946
1070	300	459	490	525	567	615	672	741	798	825	855	873	886	897	906	912	914	920	926	932	944	954
1080	300	460	492	528	569	618	676	746	804	831	861	880	893	904	913	919	921	928	934	940	952	962
1090	300	462	494	530	572	621	680	750	809	837	868	886	900	911	920	926	928	935	941	947	959	969
1100	300	464	496	532	575	625	684	755	815	843	874	893	907	918	927	933	935	943	949	955	967	977
1110	300	466	498	535	578	628	687	760	820	849	880	900	914	925	935	941	943	950	956	962	975	985
1120	300	468	500	537	580	631	691	764	825	855	886	906	920	932	942	948	950	957	964	970	982	993
1130	300	469	502	539	583	634	695	769	831	861	893	913	927	939	949	955	957	965	971	977	990	1001
1140	300	471	504	542	586	637	699	774	836	867	899	919	934	946	956	962	964	972	979	985	998	1009
1150	300	473	506	544	588	640	703	778	842	872	905	926	941	953	963	969	971	979	986	992	1005	1017
1160	300	474	508	546	591	643	706	783	847	878	911	932	947	960	970	976	979	986	993	1000	1013	1024
1170	300	476	510	548	593	646	710	787	852	884	918	939	954	966	977	983	986	993	1001	1007	1021	1032
1180	300	478	512	551	596	650	714	792	858	889	924	945	961	973	984	990	993	1001	1008	1014	1028	1040
1190	300	479	513	553	598	653	717	796	863	895	930	951	967	980	991	998	1000	1008	1015	1022	1036	1048
1200	300	481	515	555	601	656	721	801	868	901	936	958	974	987	998	1005	1007	1015	1022	1029	1043	1056

Table 5. Pixel brightness temperatures and band saturation characteristics for VIIRS band M8 (1.24 µm).

1.24 µm	A (pixel)																				
T (K)	0	1E-09	1E-08	0.0000001	0.000001	0.00001	0.0001	0.001	0.005	0.01	0.02	0.03	0.04	0.05	0.06	0.067385	0.07	0.08	0.09	0.1	0.125	0.15
800	300	330	352	379	410	446	489	542	586	607	630	644	655	663	670	675	676	681	686	690	700	707
810	300	331	354	381	412	449	493	546	591	613	636	651	661	670	677	682	683	689	693	698	707	715
820	300	333	356	383	415	452	497	551	597	619	642	657	668	677	684	689	690	696	701	705	715	723
830	300	335	358	386	417	455	500	556	602	624	649	664	675	684	691	696	697	703	708	713	723	731
840	300	336	360	388	420	458	504	560	607	630	655	670	681	690	698	703	704	710	715	720	730	739
850	300	338	362	390	422	461	508	564	612	636	661	676	688	697	705	710	711	717	723	727	738	746
860	300	339	364	392	425	464	511	569	618	641	667	683	694	704	712	717	718	724	730	735	745	754
870	300	341	365	394	427	467	515	573	623	647	673	689	701	710	718	724	725	731	737	742	753	762
880	300	342	367	396	430	470	518	577	628	652	679	695	707	717	725	731	732	739	744	749	760	769
890	300	344	369	398	432	473	522	582	633	658	685	701	714	724	732	737	739	746	751	756	768	777
900	300	345	371	400	434	475	525	586	638	663	690	708	720	730	739	744	746	753	758	764	775	785
910	300	347	372	402	437	478	528	590	643	669	696	714	727	737	746	751	753	760	765	771	782	792
920	300	348	374	404	439	481	532	594	648	674	702	720	733	743	752	758	760	767	773	778	790	800
930	300	350	376	406	441	484	535	599	653	679	708	726	739	750	759	765	767	773	780	785	797	807
940	300	351	377	408	444	486	538	603	658	685	714	732	746	756	766	771	773	780	787	792	804	815
950	300	352	379	410	446	489	542	607	663	690	720	738	752	763	772	778	780	787	794	799	812	822
960	300	354	380	411	448	492	545	611	667	695	725	744	758	769	779	785	787	794	801	806	819	830
970	300	355	382	413	450	494	548	615	672	700	731	750	764	776	785	792	794	801	807	813	826	837
980	300	356	383	415	452	497	551	619	677	706	737	756	771	782	792	798	800	808	814	820	834	845
990	300	358	385	417	454	499	554	623	682	711	742	762	777	788	798	805	807	814	821	827	841	852
1000	300	359	386	419	456	502	557	627	687	716	748	768	783	795	805	811	814	821	828	834	848	859
1010	300	360	388	420	459	504	561	631	691	721	753	774	789	801	811	818	820	828	835	841	855	867
1020	300	361	389	422	461	507	564	635	696	726	759	780	795	807	818	825	827	835	842	848	862	874
1030	300	363	391	424	463	509	567	638	701	731	765	785	801	814	824	831	833	841	849	855	870	882
1040	300	364	392	425	465	512	570	642	705	736	770	791	807	820	831	838	840	848	855	862	877	889
1050	300	365	394	427	467	514	573	646	710	741	775	797	813	826	837	844	846	855	862	869	884	896
1060	300	366	395	429	469	517	576	650	714	746	781	803	819	832	843	850	853	861	869	876	891	903
1070	300	368	396	430	471	519	579	654	719	751	786	809	825	838	850	857	859	868	876	883	898	911
1080	300	369	398	432	472	521	581	657	723	756	792	814	831	845	856	863	866	874	882	889	905	918
1090	300	370	399	434	474	524	584	661	728	761	797	820	837	851	862	870	872	881	889	896	912	925
1100	300	371	401	435	476	526	587	665	732	766	802	826	843	857	868	876	879	887	896	903	919	932
1110	300	372	402	437	478	528	590	668	737	771	808	831	849	863	875	882	885	894	902	910	926	939
1120	300	373	403	438	480	530	593	672	741	775	813	837	855	869	881	889	891	900	909	916	933	947
1130	300	374	404	440	482	533	596	676	745	780	818	842	860	875	887	895	898	907	915	923	940	954
1140	300	375	406	441	484	535	598	679	750	785	823	848	866	881	893	901	904	913	922	930	947	961
1150	300	377	407	443	485	537	601	683	754	790	829	853	872	887	899	907	910	920	928	936	953	968
1160	300	378	408	444	487	539	604	686	758	794	834	859	878	893	905	914	916	926	935	943	960	975
1170	300	379	409	446	489	541	607	690	763	799	839	864	883	899	911	920	923	933	941	950	967	982
1180	300	380	411	447	491	544	609	693	767	804	844	870	889	904	917	926	929	939	948	956	974	989
1190	300	381	412	449	492	546	612	697	771	808	849	875	895	910	924	932	935	945	954	963	981	996
1200	300	382	413	450	494	548	615	700	775	813	854	881	900	916	930	938	941	951	961	969	988	1003

Table 6. Pixel brightness temperatures and band saturation characteristics for VIIRS band M10 (1.61 µm).

1.61 µm	A (pixel)																					
T (K)	0	1E-09	1E-08	0.0000001	0.000001	0.00001	0.0001	0.001	0.005	0.01	0.02	0.03	0.04	0.05	0.06	0.067385	0.07	0.08	0.09	0.1	0.125	0.15
800	300	301	308	328	358	394	438	494	543	566	593	609	621	631	639	644	646	652	658	663	674	684
810	300	301	309	330	360	396	441	498	547	571	598	615	627	637	645	651	653	659	665	670	682	691
820	300	302	310	332	362	399	444	502	552	576	603	620	633	643	652	657	659	666	672	677	689	698
830	300	302	311	333	364	401	447	506	556	581	609	626	639	649	658	664	666	672	678	684	696	706
840	300	302	312	335	366	403	450	509	561	586	614	632	645	655	664	670	672	679	685	691	703	713
850	300	302	313	336	367	406	453	513	565	591	619	637	651	662	671	676	678	685	692	697	710	720
860	300	302	314	338	369	408	456	517	570	596	625	643	657	668	677	683	685	692	698	704	717	727
870	300	303	315	339	371	410	459	520	574	601	630	649	662	674	683	689	691	698	705	711	724	734
880	300	303	316	341	373	412	461	524	578	605	635	654	668	680	689	695	697	705	711	717	730	741
890	300	303	317	342	375	415	464	527	583	610	640	660	674	685	695	702	704	711	718	724	737	749
900	300	304	318	343	376	417	467	531	587	615	646	665	680	691	701	708	710	717	724	731	744	756
910	300	304	319	345	378	419	470	534	591	619	651	671	685	697	707	714	716	724	731	737	751	763
920	300	304	320	346	380	421	472	538	595	624	656	676	691	703	713	720	722	730	737	744	758	770
930	300	305	321	348	382	423	475	541	599	629	661	681	697	709	719	726	728	736	744	750	765	777
940	300	305	322	349	383	425	477	544	604	633	666	687	702	715	725	732	735	743	750	757	771	784
950	300	306	323	350	385	427	480	548	608	638	671	692	708	721	731	738	741	749	756	763	778	791
960	300	306	324	352	386	429	483	551	612	642	676	697	713	726	737	744	747	755	763	770	785	797
970	300	306	325	353	388	431	485	554	616	647	681	703	719	732	743	750	753	761	769	776	791	804
980	300	307	326	354	390	433	488	558	620	651	686	708	724	738	749	756	759	767	775	782	798	811
990	300	307	327	356	391	435	490	561	624	656	691	713	730	743	755	762	765	774	782	789	805	818
1000	300	308	328	357	393	437	492	564	628	660	696	718	735	749	761	768	771	780	788	795	811	825
1010	300	308	329	358	394	439	495	567	632	664	700	723	741	755	766	774	777	786	794	801	818	832
1020	300	309	330	359	396	441	497	570	636	669	705	728	746	760	772	780	783	792	800	808	824	838
1030	300	309	331	361	397	443	500	573	639	673	710	734	751	766	778	786	788	798	806	814	831	845
1040	300	310	332	362	399	444	502	577	643	677	715	739	757	771	783	792	794	804	812	820	837	852
1050	300	311	333	363	400	446	504	580	647	681	719	744	762	777	789	797	800	810	818	826	844	859
1060	300	311	333	364	402	448	507	583	651	686	724	749	767	782	795	803	806	816	825	833	850	865
1070	300	312	334	365	403	450	509	586	655	690	729	754	772	788	800	809	812	822	831	839	857	872
1080	300	312	335	366	405	452	511	589	658	694	733	759	778	793	806	815	817	827	837	845	863	879
1090	300	313	336	368	406	453	513	592	662	698	738	763	783	798	812	820	823	833	843	851	869	885
1100	300	313	337	369	407	455	516	595	666	702	742	768	788	804	817	826	829	839	849	857	876	892
1110	300	314	338	370	409	457	518	597	669	706	747	773	793	809	823	831	834	845	854	863	882	898
1120	300	315	339	371	410	458	520	600	673	710	752	778	798	814	828	837	840	851	860	869	888	905
1130	300	315	340	372	411	460	522	603	677	714	756	783	803	820	834	843	846	856	866	875	895	911
1140	300	316	341	373	413	462	524	606	680	718	761	788	808	825	839	848	851	862	872	881	901	918
1150	300	316	342	374	414	463	526	609	684	722	765	792	813	830	844	854	857	868	878	887	907	924
1160	300	317	342	375	415	465	528	612	687	726	769	797	818	835	850	859	862	874	884	893	913	931
1170	300	318	343	376	417	467	530	614	691	730	774	802	823	840	855	865	868	879	890	899	920	937
1180	300	318	344	377	418	468	532	617	694	734	778	807	828	846	860	870	873	885	895	905	926	944
1190	300	319	345	378	419	470	535	620	698	738	782	811	833	851	866	876	879	891	901	911	932	950
1200	300	319	346	379	420	471	537	623	701	742	787	816	838	856	871	881	884	896	907	917	938	956

Table 7. Pixel brightness temperatures and band saturation characteristics for VIIRS band M11 (2.25 µm).

2.25 µm	A (pixel)																				
T (K)	0	1E-09	1E-08	0.0000001	0.000001	0.00001	0.0001	0.001	0.005	0.01	0.02	0.03	0.04	0.05	0.06	0.067385	0.07	0.08	0.09	0.1	0.125	0.15
800	300	300	300	301	307	330	372	429	481	508	537	556	570	582	592	598	600	608	615	621	635	647
810	300	300	300	301	307	332	374	432	485	512	542	561	575	587	597	604	606	614	621	627	641	653
820	300	300	300	301	308	333	376	435	488	516	546	566	580	592	603	609	612	619	627	633	647	660
830	300	300	300	301	309	335	378	438	492	520	551	570	585	598	608	615	617	625	632	639	654	666
840	300	300	300	301	309	336	380	440	495	523	555	575	590	603	613	620	623	631	638	645	660	672
850	300	300	300	301	310	338	382	443	499	527	559	580	595	608	619	626	628	636	644	651	666	679
860	300	300	300	301	311	339	384	446	502	531	564	584	600	613	624	631	633	642	650	657	672	685
870	300	300	300	302	311	341	386	449	506	535	568	589	605	618	629	636	639	648	655	663	678	692
880	300	300	300	302	312	342	388	451	509	539	572	594	610	623	634	642	644	653	661	668	684	698
890	300	300	300	302	313	343	390	454	512	542	576	598	615	628	640	647	650	659	667	674	690	704
900	300	300	300	302	313	345	392	456	516	546	580	603	619	633	645	652	655	664	672	680	696	710
910	300	300	300	302	314	346	394	459	519	550	585	607	624	638	650	658	660	669	678	685	702	717
920	300	300	300	302	315	347	396	461	522	553	589	612	629	643	655	663	665	675	683	691	708	723
930	300	300	300	302	316	349	398	464	525	557	593	616	634	648	660	668	671	680	689	697	714	729
940	300	300	300	303	316	350	399	466	528	561	597	620	638	653	665	673	676	686	694	702	720	735
950	300	300	300	303	317	351	401	469	532	564	601	625	643	657	670	678	681	691	700	708	726	741
960	300	300	300	303	318	353	403	471	535	568	605	629	647	662	675	683	686	696	705	713	732	747
970	300	300	300	303	319	354	405	474	538	571	609	633	652	667	680	688	691	701	711	719	738	753
980	300	300	300	303	319	355	407	476	541	575	613	638	656	672	685	693	696	707	716	724	743	759
990	300	300	300	304	320	357	408	478	544	578	617	642	661	676	690	698	701	712	721	730	749	765
1000	300	300	300	304	321	358	410	481	547	581	621	646	665	681	695	703	706	717	727	735	755	771
1010	300	300	300	304	322	359	412	483	550	585	624	650	670	686	699	708	711	722	732	741	760	777
1020	300	300	300	304	323	360	413	485	553	588	628	654	674	690	704	713	716	727	737	746	766	783
1030	300	300	301	304	323	361	415	488	556	591	632	658	678	695	709	718	721	732	742	752	772	789
1040	300	300	301	305	324	363	416	490	559	595	636	662	683	699	714	723	726	737	748	757	777	795
1050	300	300	301	305	325	364	418	492	562	598	639	666	687	704	718	728	731	742	753	762	783	801
1060	300	300	301	305	326	365	420	494	564	601	643	671	691	708	723	733	736	747	758	767	788	807
1070	300	300	301	305	326	366	421	496	567	604	647	675	696	713	728	737	741	752	763	773	794	812
1080	300	300	301	306	327	367	423	499	570	608	651	678	700	717	732	742	745	757	768	778	800	818
1090	300	300	301	306	328	368	424	501	573	611	654	682	704	722	737	747	750	762	773	783	805	824
1100	300	300	301	306	329	370	426	503	576	614	658	686	708	726	742	752	755	767	778	788	810	830
1110	300	300	301	306	329	371	427	505	578	617	661	690	712	731	746	756	760	772	783	793	816	835
1120	300	300	301	307	330	372	429	507	581	620	665	694	716	735	751	761	764	777	788	798	821	841
1130	300	300	301	307	331	373	430	509	584	623	668	698	721	739	755	766	769	782	793	804	827	847
1140	300	300	301	307	332	374	432	511	586	626	672	702	725	743	760	770	774	786	798	809	832	852
1150	300	300	301	308	332	375	433	513	589	629	675	706	729	748	764	775	778	791	803	814	837	858
1160	300	300	301	308	333	376	434	515	592	632	679	709	733	752	768	779	783	796	808	819	843	863
1170	300	300	301	308	334	377	436	517	594	635	682	713	737	756	773	784	787	801	813	824	848	869
1180	300	300	301	309	335	378	437	519	597	638	686	717	741	760	777	788	792	805	817	829	853	874
1190	300	300	301	309	335	379	439	521	599	641	689	720	745	764	781	793	796	810	822	833	858	880
1200	300	300	301	309	336	380	440	523	602	644	692	724	749	769	786	797	801	815	827	838	864	885

Table 8. Pixel brightness temperatures and band saturation characteristics for VIIRS band M13 (4.05 µm).

4.05 µm	A (pixel)																					
T (K)	0	1E-09	1E-08	0.0000001	0.000001	0.00001	0.0001	0.001	0.005	0.01	0.02	0.03	0.04	0.05	0.06	0.067385	0.07	0.08	0.09	0.1	0.125	0.15
800	300	300	300	300	300	300	304	327	370	396	427	449	465	479	491	499	502	511	520	528	546	562
810	300	300	300	300	300	300	304	328	371	398	430	452	469	483	495	503	506	515	524	532	551	567
820	300	300	300	300	300	300	304	329	373	400	433	455	472	486	499	507	510	519	528	537	555	572
830	300	300	300	300	300	300	305	330	375	403	436	458	475	490	502	511	513	523	533	541	560	576
840	300	300	300	300	300	301	305	331	377	405	438	461	479	493	506	514	517	527	537	545	565	581
850	300	300	300	300	300	301	305	332	379	407	441	464	482	497	510	518	521	531	541	550	569	586
860	300	300	300	300	300	301	305	333	381	409	444	467	485	500	513	522	525	535	545	554	574	591
870	300	300	300	300	300	301	306	334	383	412	446	470	488	504	517	526	529	539	549	558	578	596
880	300	300	300	300	300	301	306	335	384	414	449	473	491	507	520	529	532	543	553	562	583	600
890	300	300	300	300	300	301	306	337	386	416	452	476	495	510	524	533	536	547	557	566	587	605
900	300	300	300	300	300	301	306	338	388	418	454	479	498	514	527	537	540	551	561	570	591	610
910	300	300	300	300	300	301	307	339	390	420	457	481	501	517	531	540	543	554	565	574	596	614
920	300	300	300	300	300	301	307	340	392	422	459	484	504	520	534	544	547	558	569	578	600	619
930	300	300	300	300	300	301	307	341	393	424	462	487	507	523	538	547	550	562	573	582	604	624
940	300	300	300	300	300	301	307	342	395	426	464	490	510	527	541	551	554	566	576	586	609	628
950	300	300	300	300	300	301	308	343	397	428	467	493	513	530	544	554	557	569	580	590	613	633
960	300	300	300	300	300	301	308	344	398	430	469	495	516	533	548	558	561	573	584	594	617	**637**
970	300	300	300	300	300	301	308	345	400	432	471	498	519	536	551	561	564	577	588	598	621	**642**
980	300	300	300	300	300	301	308	346	402	434	474	501	522	539	554	564	568	580	592	602	626	**646**
990	300	300	300	300	300	301	309	347	403	436	476	503	524	542	558	568	571	584	595	606	630	**651**
1000	300	300	300	300	300	301	309	348	405	438	479	506	527	545	561	571	575	587	599	610	634	**655**
1010	300	300	300	300	300	301	309	349	406	440	481	508	530	548	564	575	578	591	603	613	**638**	**659**
1020	300	300	300	300	300	301	310	350	408	442	483	511	533	551	567	578	581	594	606	617	**642**	**664**
1030	300	300	300	300	300	301	310	351	410	444	485	514	536	554	570	581	585	598	610	621	**646**	**668**
1040	300	300	300	300	300	301	310	352	411	446	488	516	538	557	573	584	588	601	613	625	**650**	**672**
1050	300	300	300	300	300	301	310	353	413	448	490	519	541	560	577	588	591	605	617	628	**654**	**677**
1060	300	300	300	300	300	301	311	354	414	450	492	521	544	563	580	591	595	608	621	632	**658**	**681**
1070	300	300	300	300	300	301	311	355	416	451	494	524	547	566	583	594	598	611	624	**636**	**662**	**685**
1080	300	300	300	300	300	301	311	356	417	453	497	526	549	569	586	597	601	615	628	**639**	**666**	**689**
1090	300	300	300	300	300	301	312	357	419	455	499	528	552	572	589	600	604	618	631	**643**	**670**	**694**
1100	300	300	300	300	300	301	312	358	420	457	501	531	555	575	592	603	607	621	**634**	**647**	**674**	**698**
1110	300	300	300	300	300	301	312	358	422	459	503	533	557	577	595	607	611	625	**638**	**650**	**678**	**702**
1120	300	300	300	300	300	302	313	359	423	460	505	536	560	580	598	610	614	628	**641**	**654**	**682**	**706**
1130	300	300	300	300	300	302	313	360	425	462	507	538	562	583	601	613	617	631	**645**	**657**	**685**	**710**
1140	300	300	300	300	300	302	313	361	426	464	509	540	565	586	604	616	620	**635**	**648**	**661**	**689**	**714**
1150	300	300	300	300	300	302	313	362	427	465	511	543	568	588	607	619	623	**638**	**651**	**664**	**693**	**718**
1160	300	300	300	300	300	302	314	363	429	467	513	545	570	591	609	622	626	**641**	**655**	**668**	**697**	**722**
1170	300	300	300	300	300	302	314	364	430	469	515	547	573	594	612	625	629	**644**	**658**	**671**	**700**	**726**
1180	300	300	300	300	300	302	314	365	432	470	517	550	575	596	615	628	632	**647**	**661**	**675**	**704**	**730**
1190	300	300	300	300	300	302	315	366	433	472	519	552	578	599	618	631	**635**	**650**	**665**	**678**	**708**	**734**
1200	300	300	300	300	300	302	315	367	434	474	521	554	580	602	621	634	**638**	**654**	**668**	**681**	**712**	**738**

Table 9. Pixel brightness temperatures and band saturation characteristics for VIIRS band M15 (10.76 μm).

10.8 μm	A (pixel)																					
T (K)	0	1E-09	1E-08	0.0000001	0.000001	0.00001	0.0001	0.001	0.005	0.01	0.02	0.03	0.04	0.05	0.06	0.067385	0.07	0.08	0.09	0.1	0.125	0.15
800	300	300	300	300	300	300	300	301	306	312	323	333	342	351	360	366	368	376	383	391	408	424
810	300	300	300	300	300	300	300	301	306	312	323	334	343	352	361	367	369	377	385	393	410	427
820	300	300	300	300	300	300	300	301	306	312	324	334	344	354	362	369	371	379	387	394	412	429
830	300	300	300	300	300	300	300	301	307	313	324	335	345	355	364	370	372	381	389	396	415	432
840	300	300	300	300	300	300	300	301	307	313	325	336	346	356	365	372	374	382	390	398	417	434
850	300	300	300	300	300	300	300	301	307	313	326	337	347	357	366	373	375	384	392	400	419	437
860	300	300	300	300	300	300	300	301	307	314	326	338	348	358	368	375	377	386	394	402	421	440
870	300	300	300	300	300	300	300	301	307	314	327	338	349	359	369	376	378	387	396	404	424	442
880	300	300	300	300	300	300	300	302	307	314	327	339	350	361	370	377	380	389	398	406	426	445
890	300	300	300	300	300	300	300	302	308	315	328	340	351	362	372	379	381	391	399	408	428	447
900	300	300	300	300	300	300	300	302	308	315	328	341	352	363	373	380	383	392	401	410	430	450
910	300	300	300	300	300	300	300	302	308	315	329	342	353	364	374	382	384	394	403	412	433	452
920	300	300	300	300	300	300	300	302	308	316	330	342	354	365	376	383	386	395	405	414	435	455
930	300	300	300	300	300	300	300	302	308	316	330	343	355	366	377	385	387	397	406	415	437	457
940	300	300	300	300	300	300	300	302	308	316	331	344	356	368	378	386	389	399	408	417	439	460
950	300	300	300	300	300	300	300	302	309	317	331	345	357	369	380	388	390	400	410	419	441	462
960	300	300	300	300	300	300	300	302	309	317	332	345	358	370	381	389	392	402	412	421	443	464
970	300	300	300	300	300	300	300	302	309	317	332	346	359	371	382	390	393	403	413	423	446	467
980	300	300	300	300	300	300	300	302	309	317	333	347	360	372	384	392	395	405	415	425	448	469
990	300	300	300	300	300	300	300	302	309	318	334	348	361	373	385	393	396	407	417	427	450	472
1000	300	300	300	300	300	300	300	302	309	318	334	349	362	374	386	395	397	408	419	428	452	474
1010	300	300	300	300	300	300	300	302	310	318	335	349	363	376	388	396	399	410	420	430	454	477
1020	300	300	300	300	300	300	300	302	310	319	335	350	364	377	389	397	400	411	422	432	456	479
1030	300	300	300	300	300	300	300	302	310	319	336	351	365	378	390	399	402	413	424	434	458	481
1040	300	300	300	300	300	300	300	302	310	319	336	352	366	379	391	400	403	414	425	436	461	484
1050	300	300	300	300	300	300	300	302	310	320	337	352	367	380	393	402	405	416	427	438	463	486
1060	300	300	300	300	300	300	300	302	310	320	338	353	368	381	394	403	406	418	429	439	465	489
1070	300	300	300	300	300	300	300	302	311	320	338	354	369	382	395	404	407	419	430	441	467	491
1080	300	300	300	300	300	300	300	302	311	321	339	355	370	383	396	406	409	421	432	443	469	493
1090	300	300	300	300	300	300	300	302	311	321	339	356	371	385	398	407	410	422	434	445	471	496
1100	300	300	300	300	300	300	300	302	311	321	340	356	372	386	399	408	412	424	435	447	473	498
1110	300	300	300	300	300	300	300	302	311	322	340	357	372	387	400	410	413	425	437	448	475	500
1120	300	300	300	300	300	300	300	302	311	322	341	358	373	388	402	411	414	427	439	450	477	503
1130	300	300	300	300	300	300	300	302	312	322	341	359	374	389	403	412	416	428	440	452	479	505
1140	300	300	300	300	300	300	300	302	312	323	342	359	375	390	404	414	417	430	442	454	481	507
1150	300	300	300	300	300	300	300	302	312	323	343	360	376	391	405	415	419	431	444	455	483	510
1160	300	300	300	300	300	300	300	303	312	323	343	361	377	392	406	416	420	433	445	457	485	512
1170	300	300	300	300	300	300	300	303	312	324	344	362	378	393	408	418	421	434	447	459	487	514
1180	300	300	300	300	300	300	300	303	312	324	344	362	379	394	409	419	423	436	448	461	489	516
1190	300	300	300	300	300	300	300	303	313	324	345	363	380	396	410	420	424	437	450	462	491	519
1200	300	300	300	300	300	300	300	303	313	324	345	364	381	397	411	422	425	439	452	464	493	521

The VIIRS SRD categorizes the Active Fires Application as "Category IIB." The "II" indicates that the threshold requirements are allowed to drive the VIIRS design, balanced against cost, so long as the manifestation of these requirements does not endanger the quality of the Category I EDRs, namely Sea Surface Temperature (SST) and Imagery. The "B" indicates that the objective requirements should not be allowed to drive the design in any significant way.

These prioritizations have led to the current, optimized VIIRS design, which provides the best value among over two dozen EDRs, but must do so at the expense of some EDR-specific specialization in the hardware, particularly when SST or Imagery is traded against another product. Since both SST and Imagery utilize the VIIRS LWIR bands, none of these bands can be driven high enough to provide coverage of the entire fire temperature/area measurement range. The best that can be done is M15, summarized in Table 9. Clearly, this band saturates for over half of the temperature/area measurement range, and therefore cannot be utilized for quantitative retrievals of temperature and area in all cases. Increasing the saturation temperature in M15 would cause the quantization to noise ratio (QNR) to become larger than 1, which has already proven to be a problem for the SST community with regard to the MODIS Protoflight Model (PFM), as that 11 μm band has a saturation temperature of 400 K because of the MODIS fire requirements. The MODIS Flight Model 1 (FM1), to be carried on Aqua, has a much lower saturation temperature for this reason, and the same has been done for the VIIRS design. The thermal imagery band on VIIRS—I5—is a key band for the Imagery EDR, and therefore also does not possess enough flexibility to solve this dilemma.

Consequently, the VIIRS Active Fires algorithm must provide a data processing solution to handle the saturation of the LWIR band. The approach adopted late in Phase I algorithm development was to activate several NIR/SWIR bands at night, so that these bands could be used together with M13—which has been designed to cover the full fire temperature/area measurement range—in instances where M15 saturates, both day and night. More detail on this approach is provided in Section 3.3.2.3.

3.3.1.2 Historical Development of Fire Products

Matson and Dozier (1981) showed that simultaneous use of the 3.8 μm and 11 μm channels provides the capability to detect high temperature sources such as steel plants and waste gas flares, with the 3.8 μm channel particularly sensitive to such targets. Matson *et al*. (1984) determined that one can utilize the temperature difference between the two bands to calculate the area and temperature of a hot target. This alone does not guarantee that a fire has been detected, but the transient nature of fires can be used to screen out industrial areas, as the latter subsist from one snapshot of a given location to the next.

In an effort to begin characterizing the background environment surrounding a fire, Matson and Holben (1987) investigated the use of the NDVI in addition to the MWIR-LWIR temperature difference, and they found it to show good promise for burn scar detection and other similar phenomena.

One of the challenges facing the early development of fire detection techniques was the difficulty in applying any one algorithm globally. Until the past decade or so, most fire detection techniques were simple threshold tests with the brightness temperatures and brightness temperature differences in the available channels. This approach must be applied differently in forests than in savannas. The former tend to provide a relatively cooler environment for fires than the latter, and any threshold optimized for one scenario will fail somewhat for the other. In an attempt to surmount this problem, Franca *et al*. (1995) developed a multispectral methodology based on NOAA-11 AVHRR data, to at least partially resolve the numerous problems with error sources such as large surface heterogeneity, clouds, smoke, haze, background emissivities, and so forth. Their technique obtained more realistic results, and did not overestimate or underestimate the number of fires sensible by the satellite. This particular algorithm seems to work fairly well in both savanna and forest environments. It starts with the identification of candidate pixels using the channel 3 (3.7 μm) threshold of saturation, around 320 K. Vickos (1991) showed when there is no ambiguity between fire and its environment, this test alone is sufficient. The Franca algorithm subsequently computes the brightness temperature difference between channels 3 and 4, ΔT_{34}, to check for cloud effects. A second difference between AVHRR channels 4 and 5, ΔT_{45}, is applied to account for additional cloud effects. ΔT_{34} tends to provide better separation of fires, whereas ΔT_{45} allows fairly robust separation of fires from clouds.

Harris (1996) derived a different approach, helping to signal a new paradigm for active fire detection. Rather than applying straight thresholds, the algorithm attempts to develop a context for the candidate pixel in question. The algorithm is applied to an image of ΔT_{34}. First, it calculates the difference between the center pixel and its immediate background, $\Delta(\Delta T_{34})$. The immediate background is defined by centering a 3x3 pixel window on the target pixel and taking the mean of ΔT_{34} for the eight surrounding pixels. $\Delta(\Delta T_{34})$ is then compared with the subimage natural variation, which is defined as the maximum $\Delta(\Delta T_{34})$ for a fire-free portion of the subimage. This fire-free portion is in turn defined by a fire-screened 45x45 km area taken from top NE corner of the subimage. Fire screening is conducted by rejecting pixels detached from the natural variation frequency distribution tail. If $\Delta(\Delta T_{34})$ is greater than the natural variation, the pixel is flagged. About 22% false alarms were found with this approach, caused primarily by industrial sources or clouds.

The transition to contextual fire detection was completed with Flasse and Ceccato (1996). Placed in contrast with threshold techniques, their algorithm uses pixels in the immediate neighborhood to derive a localized context for fire detection that is self-adaptive and consistent over large areas and through different seasons. The algorithm has been successfully tested in most areas of world. It works well because it is relative instead of absolute in nature, so that hot savanna fires can be detected just as robustly as cooler forest fires without adjusting thresholds. There are two stages to the algorithm: selecting candidate pixels (potential fires, PFs), and then confirming or rejecting the pixel based on the behavior of its immediate neighbors. A pixel is selected as a PF if $T_3 > 311$ K and $\Delta T_{34} > 8$ K. The low threshold for the first test is set to avoid rejection of cooler fires. A second test eliminates pixels where the reflectance in the near IR channel, ρ_2, is greater than or equal to 20%. This allows some screening of sunglint, bright soil, and clouds.

The second stage of the Flasse and Ceccato algorithm works as follows. For each PF, statistics are calculated for a variable sized context window (from 3x3 up to 15x15 pixels) around the PF. The size of the window hinges upon having at least 25% of the neighboring pixels as background, and at least three pixels must be eligible for the computation. If these conditions are not met, the PF is rejected. Otherwise, the following quantities are computed:

T_{3b}, the mean of the channel 3 brightness temperature T_3 for the fire background

σ_{T3b}, the standard deviation of the channel 3 brightness temperature for the fire background

T_{34b}, the mean of the difference between the channel 3 and channel 4 brightness temperatures, T_3 and T_4 for the background

σ_{T34b}, the standard deviation of the difference between the channel 3 and channel 4 brightness temperatures for the background

Finally, the contextual test is applied. A PF is confirmed to be a fire when

$$T_{3PF} - (T_{3b} + 2\sigma_{T3b}) > 3\text{ K}$$

and

$$T_{34PF} > T_{34b} + 2\sigma_{T34b}$$

The success of contextual fire detection methods in recent years has led to the adoption of the methodology for the MODIS Fire Products, described in Kaufman and Justice (1998). Briefly, the MODIS fire detection algorithm works as follows:

1) Cloud detection and scan angle. The MODIS cloud mask and a 45 degree scan angle cutoff are used to disqualify pixels for subsequent processing.

2) Atmospheric correction. The brightness temperatures in the 4 µm and 11 µm bands, T_4 and T_{11}, respectively, are corrected for gaseous absorption.

3) Background characterization. This follows Flasse and Ceccato (1996), only it allows the window to be sized as large as 21x21 pixels. Energetic fire pixels are eliminated from analysis if $T_{41} = T_4 - T_{11} \geq 20$ K (10 K at night) and $T_4 > 320$ K (315 K at night). If these tests are passed, then the statistical parameters T_{11b}, δT_{11}, T_{4b}, δT_4, T_{41b} and δT_{41} are calculated, where the subscript b denotes a mean and the prefix δ denotes a standard deviation.

4) Fire detection. If $T_4 < 315$ K (305 K night) or $T_{41} < 5$K (3K at night), the pixel is rejected. If δT_4 and δT_{41} are less than 2K, they are set to 2K. The pixel defined to contain an active fire if following conditions are met:

   $\{[(T_4 > T_{4b} + 4\delta T_4)$ or $T_4 > 320$ K (315K at night)] and

   $[(T_{41} > T_{41b} + 4\delta\Delta T_{41})$ or $T_{41} > 20$ K (10K at night)]$\}$

   or $\{T_4 > 360$ K (330 K at night) $\}$

5) Glint exclusion. A fire pixel is excluded during the day if the reflectance in the red band, $\rho_{0.64}$, is greater than 0.3 and the reflectance in the near IR band, $\rho_{0.86}$, is greater than 0.3, and the glint angle is less than 40 degrees. This is the end of MODIS Level 2 processing

for fires. Further processing is MODIS-specific and targets the emitted energy, as well as identification of the smoldering/flaming stage.

Raytheon has built some heritage with fire detection recently as part of efforts with the Hazard Support System (HSS). Raytheon (1998) summarizes the trades that went into the selection of fire detection algorithms for the HSS. These trades are summarized in Table 6.

Because of its clear advantages over older threshold techniques, the contextual analysis approach was adopted by Raytheon for the HSS. Two algorithms were selected, one based on Prins and Menzel (1992), Flasse and Ceccato (1996), and reported in Justice in Dowty (1993), and the other based on a similar approach developed at NASA/GSFC for use with AVHRR 1 km data. The primary algorithm proceeds in the following sequence:

1) Geolocation

2) Calibration

3) Cloud masking (using Saunders and Kriebel (1988) for AVHRR, Prins and Menzel [1996b] for GOES)

4) Threshold fire test

5) Sunglint rejection

6) Contextual fire detection

For the threshold fire test, it was recommended that values be defined by month, and that a weekly NDVI product be incorporated for background characterization. The sunglint rejection uses red and near IR reflectances, much in the same manner as for MODIS. The contextual fire detection uses windows ranging in size from 3x3 to 15x15 pixels.

Table 10. Algorithm trades conducted by Raytheon for the Hazard Support System (HSS).

Author of Algorithm (Year)	Type	Reported Performance
Matson and Dozier (1981)	Fixed threshold	Detection of steel mills and oil field gas flares. Wildfire detection not part of experiment.
Flannigan and Vonder Haar (1986)	Fixed threshold	AVHRR fire detection success: 80% not obstructed by cloud or smoke. Fires under 10 acres detected 12-14% of the time.
Kaufman *et al*. (1990)	Fixed threshold	AVHRR false positives: 10% (Melinotte and Arino, 1995)
Setzer and Pereira (1991)	Fixed threshold	AVHRR fire detection success: 96% of detected fires were verified and no reports of missing fires.
Lee and Tag (1989)	Lee and Tag	Unknown
Prins and Menzel (1992)	Spatial analysis	Unknown
Justice and Dowty (1993)	Spatial analysis	AVHRR fire detection success: 37.5% (Elvidge *et al*. 1997)
Flasse and Ceccato (1996)	Spatial analysis	AVHRR false positives: 15% (Flasse and Ceccato, 1996). AVHRR fire detection success: 37.5% (Elvidge *et al*. 1997)
Prins *et al*. (1996)	Spatial analysis	GOES 8 fire detection success: 22.2% (Elvidge *et al*. 1997). Minimum size fire detected: 10 acres.

3.3.2 Mathematical Description of VIIRS Approach

3.3.2.1 Fire Detection

The baseline VIIRS fire detection algorithm is an extension of the MODIS contextual analysis heritage. It proceeds as follows:

1) *Calibration and Geolocation*. The VIIRS Build SDR Module generates the Calibrated TOA Brightness Temperatures Sensor Data Record (SDR), which includes TOA brightness temperatures for all bands relevant to Active Fires. This SDR also includes appended geolocation and solar/viewing geometry information for each pixel. We thus have the TOA brightness temperatures in bands M13 and M15—T_{13}^* and T_{15}^*, respectively. If either band is saturated, the corresponding TOA brightness temperature is set to the saturation brightness temperatures in that band.

2) *Surface Type, Cloud, and Sunglint Masking*. If the Surface Type EDR indicates the pixel is water, permanent snow/ice, or urban, processing ceases. The VIIRS Cloud Mask IP is checked for the presence of cloud or sunglint. If the relevant individual tests categorized

the pixel as definitely clear, processing continues to Step 3. If the relevant individual tests categorized the pixel as definitely cloudy and not thin cirrus, processing ceases, and all Active Fires fields are filled with predefined "missing" values. If the relevant individual test categorized the pixel as probably clear or probably cloudy, processing continues, and the Land Quality Flag (LQF) output will indicate possible obscuration by cloud. The performance specification is not guaranteed in that case. If the relevant individual tests categorized the pixel as contaminated by correctable thin cirrus, a thin cirrus correction will be applied to generate new values of T_{13}^* and T_{15}^*, and processing continues, with the pixel flagged by the LQF output, and the performance specification is not guaranteed. If the Cloud Mask categorizes the pixel as contaminated by sunglint, processing ceases.

3) *Atmospheric Correction*. NCEP column water vapor (and possibly some source of column CO_2, a topic to be explored in later versions of this ATBD) are used to correct T_{13}^* and T_{15}^* to surface brightness temperatures T_{13} and T_{15}.

4) *Identification of Potential Fires*. Let $\Delta_{35} = T_{13} - T_{15}$. If $T_{13} < T_{min}$ or $\Delta_{35} < \Delta_{min}$, then the pixel is rejected. Otherwise, the pixel potentially contains a fire and processing continues. The baselines for T_{min} and Δ_{min} are yet to be determined; the MODIS values cannot be assumed as starting points, because the VIIRS bands have different spectral and spatial characteristics.

5) *Background Characterization*. A WxW pixel window is generated around the pixel in an attempt to construct a background characterization. This window may range from W_{min}xW_{min} up to W_{max}xW_{max} pixels in size. The current baselines for W_{min} and W_{max} are 3 and 21, respectively. At least f_{min} of the neighboring pixels must qualify as background, where f_{min} is in percent. At least N_{min} of the neighboring pixels must qualify as background. The current baselines for f_{min} and N_{min} are 25% and 3, respectively. A pixel qualifies as background if it is not a potential fire pixel (using the criteria of Step 4), is not contaminated by cloud (as defined in Step 2; thin cirrus and atmospheric corrections are also applied to background pixels), and is of the same surface type as the central pixel under consideration (information supplied by the Surface Type EDR). For any pixel in which either band is saturated, the corresponding brightness temperature is set to the saturation temperature for that band. If the f_{min} and N_{min} criteria cannot be met, the pixel is rejected. If the f_{min} and N_{min} criteria are met, the following statistical quantities are computed for all background pixels: the mean brightness temperatures in M13 and M15, denoted by μ_{13} and μ_{15}, respectively; the standard deviations in the brightness temperatures in M13 and M15, denoted by σ_{13} and σ_{15}, respectively; the mean difference between the brightness temperatures in M13 and M15 ($T_{13} - T_{15}$), denoted by μ_{35}; and the standard deviation of the difference between the brightness temperatures in M13 and M15, denoted by σ_{35}.

6) *Fire Detection*. The pixel is defined to contain an active fire if one of the following two conditions applies:

    a. $[(T_{13} > \mu_{13} + 4\sigma_{13})$ or $(T_{13} > T_{crit})]$ and $[(\Delta_{35} > \mu_{35} + 4\sigma_{35})$ or $(\Delta_{35} > \Delta_{crit})]$

    b. $T_{13} > T_{abs}$

The quantities T_{crit}, Δ_{crit}, and T_{abs} are still to be determined (TBD) during the course of VIIRS algorithm development.

3.3.2.2 Subpixel Average Fire Temperature (SAFT) and Subpixel Fire Area (SFA)

Once a pixel has been categorized as containing an active fire by the technique summarized in Section 3.3.2.1, computation of subpixel average fire temperature (SAFT) and subpixel fire area (SFA) commences. The technique for computing SFA and SAFT is an extension of that introduced by Dozier (1981), using modifications suggested by Giglio and Kendall (2000).

The spectral radiance at the top of the atmosphere can be approximately represented as:

$$\begin{aligned} R_\lambda &= f\left[\varepsilon_\lambda \tau_\lambda B_\lambda(T_{fire}) + path\_R_\lambda\right] + (1-f)\left[\varepsilon_\lambda \tau_\lambda B_\lambda(T_{bg}) + path\_R_\lambda\right] \\ &= \varepsilon_\lambda \tau_\lambda \left[f B_\lambda(T_{fire}) + (1-f) B_\lambda(T_{bg})\right] + path\_R_\lambda \end{aligned} \tag{1}$$

where

f : fraction of pixel covered by fire;

ε_λ : surface emissivity at the wavelength λ;

τ_λ : atmospheric transmittance at the wavelength λ from the surface to the top of the atmosphere;

B_λ : Planck function at the wavelength λ;

T_{fire} : the temperature of the active fire;

T_{bg} : the surface temperature of the background ;

$path\_R_\lambda$: path radiance, contributed by the atmosphere.

Theoretically, two equations formed by satellite measurements for two bands located at 4.05 µm and 10.76 µm can facilitate the measurement of subpixel fire area and temperature, so long as we borrow information from neighboring pixels for the characterization of the background. In order to do so, we must reduce the number of unknowns in (1) to two, yielding a system of two equations that can be solved for two unknowns. In the strictest sense, (1) abounds with unknowns. The fire fraction *f*, the spectral emissivity ε_λ, the atmospheric transmittance τ_λ, the fire temperature T_{fire}, the background temperature T_{bg}, and the path radiance $path\_R_\lambda$ are all unknown parameters. The key is to make several assumptions, combined with the attempted retrieval of the remaining parameters not fully addressed by the assumptions.

The two parameters being sought are *f* and T_{fire}. These are therefore assumed to remain unknown in the simplification of (1). A hidden assumption in (1) is that spectral emissivity ε_λ is the same for both the fire and the background. A fire with sufficient path length through the flames will indeed behave much like a blackbody, and in the LWIR most surfaces have an emissivity very close to 1. But in the MWIR, some surfaces depart substantially from blackbody behavior, as seen in Figure 9. Most prominent is the behavior of soil. This has significant implications for brush or agricultural fires, where a substantial soil signal is present in the weighted surface emissivity. In an attempt to account for the variability of emissivity, the VIIRS algorithm will incorporate the Surface Type EDR to allow a refinement of the emissivity estimate for M13 and M15. This essentially converts ε_λ into a known parameter, albeit with some level of error. Estimates of this error will be presented in a later version of this ATBD.

The primary gases affecting τ_λ are water vapor and carbon dioxide. Water vapor is by far the more important of these two gases, having a substantial effect on the radiances in both M13 and M15. Carbon dioxide primarily affects M13, but the degree to which this alters the TOA radiances has not yet been comprehensively measured in the VIIRS algorithm development effort. If further sensitivity studies indicate a strong dependence on column CO2, which of course will be more volatile in regions associated with biomass burning, an attempt may be made to incorporate a corresponding input into the VIIRS fire temperature/area measurement algorithm. For the present, water vapor is considered the only significant parameter. This information will be incorporated via the operational NCEP. These data will be used to determine τ_λ and convert it into another known parameter, with some associated level of error in the measurement.

Path radiance is caused by two principal effects: atmospheric scattering of downwelling and upwelling radiation, and atmospheric emission. An assumption is made for the VIIRS algorithm that neither of these is significant compared to the dominant signal in the MWIR or LWIR. In the LWIR, the background signal is expected to be much larger than the path radiance. In the MWIR, the fire signal is expected to be much larger than the path radiance. Complications arise when the LWIR saturates, and the algorithm must switch to the SWIR. This and other issues with using SWIR data will be discussed in Section 3.3.2.3. When the LWIR signal is unsaturated, however, the path radiance is considered negligible and is therefore ignored.

This leaves three unknowns in the system of equations represented by (1): f, T_{fire}, and T_{bg}. Following Dozier (1981), we assume that T_{bg} can be determined from surrounding, non-fire pixels. The VIIRS Surface Type EDR will allow us to use only surrounding pixels with the same surface type as the central pixel for retrieving T_{bg}. This will allow for substantial reduction in the errors associated with T_{bg}, some of which are discussed in Giglio and Kendall (2000). The result is an set of two equations with two unknowns—f and T_{fire}. A number of different numerical approaches can be used to solve these equations; the exact choice will be presented in Version 5 of this ATBD.

3.3.2.3 Saturation Handling

As is clear from Table 9, a significant portion of the fire temperature/area measurement range will saturate band M15. In these instances, fire detection is still viable, but temperature and area measurement become much more difficult. As was discussed in Section 3.3.1.1, it was not possible to mitigate this problem within the best-value system optimization solution for VIIRS. The burden therefore falls upon the algorithm to circumvent the saturation of M15 and still deliver estimates of fire temperature and area.

Late in Phase I algorithm development, the algorithm team worked with the sensor team to implement a hardware solution that might eventually yield a workaround in instances where M15 saturates. Specifically, the sensor specification calls for the activation of bands M7, M8, M10, and M11 both day and night. Let us now consider what occurs in these bands when band M15 saturates, moving from longer wavelengths to shorter ones.

M15 saturates at a TOA brightness temperature of 343 K (Ignoring the 20% overhead applied in the sensor design process). From Table 9, one can get a sense of what combinations of fire temperature and area cause this to happen, ignoring atmospheric attenuation. It is immediately apparent from Table 7 that band M11 does not help much in this situation. As a result, the importance of M11 has dropped substantially in the development of the Active Fires algorithm. M13, on the other hand, has been specifically designed to cover the entire temperature/area measurement range. This was possible because of the tractability of dual gain in the SWIR/MWIR focal plane. This tractability does not exist in the LWIR.

Now consider the data in Table 6, for band M10 (1.61 μm). In this band, saturation occurs for larger fires than for M15, although for smaller fires with very high temperatures, saturation actually occurs earlier in M10. In these instances, one would switch to band M8 (1.24 μm), which covers almost the entire measurement range. The strategy would be to use M13 as a pivot point. For fires that do not saturate M15, M13 and M15 would be used in (1) to derive f and T_{fire}. For fires that saturate M15, M13 would become the longer-wavelength band in (1), and M10 would become the shorter-wavelength band, until M10 saturates. At that point, the algorithm would switch to M8. For the most extreme cases, M7 (865 nm) would be used.

There are three significant hurdles to overcome with this new approach to fire temperature and area measurement. First, the system of equations in (1) becomes more unstable when the LWIR is abandoned, because most of the information in both bands being considered originates in the fire, and not in the background. Second, the scattering contributions to the path radiance become more significant the shorter the wavelength of the bands used in (1), causing the assumption that this term can be neglected to break down. Third, daytime retrievals will be contaminated by a solar reflective signal in the NIR and SWIR, and terminator orbit retrievals will be affected by a solar reflectance contribution that, while small, is significantly more difficult to pin down. If these three problems can be overcome algorithmically, the NIR/SWIR mitigation strategy for saturation in the LWIR should yield very useful measurements of f and T_{fire}. Whether these measurements are of sufficient quality to meet the EDR specifications remains to be proven.

To mitigate the increased effects of scattering in the SWIR and NIR, a climatological aerosol optical thickness correction might prove quite useful. During the day, the VIIRS Aerosol Optical Thickness EDR will be based in part on the radiance contaminated by the fire, rendering it unreliable as a correction source. At night, a direct measurement of optical thickness is not available. Persistence from the daytime measurements of aerosols might prove more robust than a climatology. Neither effect will account for aerosols associated with the burning itself.

To mitigate the effects of the solar reflective signal, the Gridded Monthly Mean Reflectance IP will be utilized, in combination with the solar/viewing geometry for the pixel in question. The errors inherent in this process have not yet been explored.

To address the issue of mathematical instability in the system of equations represented by (1), it may be worthwhile to incorporate more than two bands into the calculation. Both M7 and M8 cover most of the fire/temperature area measurement range without saturation. In fact, recent updated flowdown for band saturation in M8 will likely cause it to cover the entire measurement range without saturation. This may allow the simultaneous usage of M7, M8, and M13 in (1) whenever M15 saturates. Whether this adds sufficient stability to the calculations is unclear, but it might also allow for better handling of path radiance.

3.3.2.4 Burn Scar Detection

Raytheon proposes to consider the addition of another parameter to the Active Fires output—burn scar detection. The spectral data and EDR products needed for this activity are already available in the VIIRS system, e.g., in the Vegetation Index and Surface Type EDRs and the large number of spectral bands in the reflected solar wavelengths. If this parameter is added to the Active Fires Application, it will be described in more detail in Version 5 of this ATBD.

3.4 ALGORITHM SENSITIVITY STUDIES

Because of the late arrival of the Active Fires product into the VIIRS requirements, and also because of its relative prioritization against other VIIRS EDRs, detailed sensitivity studies are still pending as a Phase II task. This activity will draw heavily upon the MODIS validation and verification infrastructure, to allow for a low-risk, low-cost system solution to be developed for VIIRS. Some information can be gleaned from simulations, however the behavior of real fires is difficult to emulate in an artificial environment. Sensitivity studies will be targeted toward the error sources identified and described in the following subsections.

3.4.1 EDR Requirements

Table 11 lists the requirements specified by the Integrated Program Office (IPO) for the Active Fires product. The threshold requirements have been adopted as the VIIRS system specification for Active Fires. The meeting of these specifications is carried as a moderate risk at this writing, pending verification of the algorithm performance using real and simulated data in Phase II and beyond.

Raytheon is currently considering a formal request to loosen the lower bound on the area measurement range, possibly from 100 m2 to 1000 m2, based on discussions with NASA and NOAA fire detection/measurement experts. As of this writing, the issue has not been resolved; its eventual resolution will be addressed in Version 5 of this ATBD.

Table 11. VIIRS SRD prescribed requirements for the Active Fires product (TBD=to be determined; TBR=to be reviewed).

SRD Parameter No.	Parameter	Threshold	Objective
	a. Horizontal Cell Size		
N/A	1. At nadir	1 km (TBR)	0.5 km (TBR)
N/A	2. Worst case	2 km (TBR)	0.5 km (TBR)
N/A	b. Horizontal reporting interval	(TBD) (gapless or near gapless coverage of land areas required)	(TBD) (gapless or near gapless coverage of land areas required)
N/A	c. Horizontal coverage	Land	Land
	d. Measurement range		
N/A	1. Sub-pixel average temperature of active fire	800 K – 1200 K	800 K – 1200 K
N/A	2. Sub-pixel area of active fire	From 100 m^2 to 50 m by greater of pixel in-scan and in-track dimensions (TBR)	From 50 m^2 to 100 m by greater of pixel in-scan and in-track dimensions (TBR)
	e. Measurement Uncertainty		
N/A	1. Sub-pixel average temperature of active fire	50 K (TBR)	25 K (TBR)
N/A	2. Sub-pixel area of active fire	30% (TBR)	15% (TBR)
N/A	f. Mapping Uncertainty	0.2 km (TBR)	0.1 km
N/A	g. Maximum local average revisit time	6 hrs	1 hr
N/A	h. Maximum local refresh	(TBD)	(TBD)
N/A	i. Minimum swath width (all other EDR thresholds met)	3000 km (TBR)	(TBR)

3.4.2 Performance Metrics

The SRD requirements set the limits for an error budget in the Active Fires product. There is one key parameter in Table 11 that directly constrains the allowable errors in the Active Fires product: uncertainty, both for subpixel fire temperature and subpixel fire area. Appendix A of the VIIRS SRD defines the uncertainty metric for assessment of EDR algorithm performance.

Consider a single true value T of an EDR product at the HCS. A satellite-borne sensor will produce data which can be transformed through a retrieval algorithm into an estimate X_i of T, where the index i indicates that any arbitrary number N of such estimates can be made. Various error sources along the pipeline between the true value T and the measured value X_i will cause X_i to deviate from T.

The uncertainty U_{SRD} is defined in the VIIRS SRD as:

$$U_{\mathrm{SRD}} = \left(\frac{1}{N} \sum_{i=1}^{N} \left(X_i - \mu \right)^2 \right)^{\frac{1}{2}} \tag{2}$$

The uncertainty is therefore alternatively known as the root mean square (RMS) error between the measurements X_i and the true value T.

As mentioned in the SRD, the definition of uncertainty given in (2) is idealized, because it assumes a single value of T. In reality, (2) cannot be implemented, because there is an infinite number of possible values for T, each possible value is likely to be manifested as truth only once, and we cannot hope to pinpoint T to arbitrary accuracy.

The practical implementation of the SRD definition is to bin the possible values of T into small ranges that are large enough to provide a statistically significant number of test points, but small enough not to be dominated by natural variability. The simplest result is a modification of (2) into the following:

$$U = \left(\frac{1}{N} \sum_{i=1}^{N} (X_i - T_i)^2 \right)^{\frac{1}{2}} \tag{3}$$

Thus, the single value of T in the SRD uncertainty definition is now changed to the particular true value T_i corresponding to the measurement X_i. Equation (3) now exactly corresponds to the RMS error. This is a common statistical measure of algorithm performance. Interestingly, only the fire temperature and area are constrained by uncertainty requirements. No quality metric is assigned to fire detection. Were such a metric in place, it would best be couched in terms of a correct typing probability, similar to that for Surface Type or Snow Cover. In future versions of this ATBD, fire detection performance will be gauged in these terms for completeness.

3.4.3 Individual Error Sources for Investigation

The Active Fires product is subject to several sources of error. The sensitivity of the algorithm to these error sources was not explored in detail in Phase I, however they can be identified and briefly described here. Phase II algorithm development efforts will center around an assessment of these error sources in the context of the algorithm described in Section 3.3.

Sensor Errors

There are several key parameters associated with the VIIRS instrument that affect its ability to facilitate sound fire retrievals. These include calibration, sensor noise, saturation, spectral content, geolocation, MTF effects, and band to band registration. Calibration will be handled post-launch via monitoring of gas flares, in much the same way MODIS is approaching the problem. Sensor noise in the VIIRS spectral bands is minimal due to the stringent requirements for Aerosol, Surface Temperature, and Ocean Color EDRs. Saturation has already been discussed at length. Spectral content is superb for VIIRS; the reflectance-based bands that will be active at night are hoped to provide a new level of capability for temperature and area computations. Geolocation and misregistration effects should be minimal due to the driving requirements for other EDRs, especially NDVI and Snow Cover, but coregistration is extremely important for fire retrievals, and so this issue must be thoroughly explored for the Active Fires EDR. VIIRS will employ the MODIS/Landsat geolocation algorithm, which exhibits excellent performance after post-launch calibration. MTF effects in the imagery bands will be minimized by the Imagery EDR requirements, however these are not used in the baseline Active Fires algorithm. The MTF performance of the moderate resolution bands is somewhat looser, which actually helps from a saturation standpoint, but it also smears the signal being measured. This is particularly important in the presence of clouds. Each of these effects will be gauged and monitored as the VIIRS design evolves into fabrication in Phase II and beyond, and the results will be recorded in future versions of this document.

Cloud Contamination

The presence of clouds can cause spurious signals in the MWIR that appear as fires if not properly accounted for. Threshold techniques are very sensitive to these effects. The VIIRS algorithm will benefit from a wealth of spectral data that are expected to minimize this error, and the VIIRS Cloud Mask is expected to be quite accurate by the time the first VIIRS is flown, because of the tremendous advances being made in cloud masking using MODIS data. At the least, the robustness of the "confident clear" category should be quite good for VIIRS, and this is the only category for which Active Fires performance is guaranteed. Performance in other situations will be evaluated as opportunities arise for a mature assessment.

Smoke

It seems at first amusing that the Active Fires product cannot be retrieved for pixels obscured by smoke. The problem is real and straightforward, however: if the surface cannot be seen, then the fire temperature and area cannot be calculated, nor can a fire even be detected for certain. From an operational standpoint, the smoke itself will raise a flag on its own. It must also be remembered that most fires occur in the presence of strong winds, and indeed if one surveys the large number of satellite images containing fires, the corresponding smoke plumes are almost always blown great distances in some direction away from the fire, exposing the active core of the fire itself. Still, some haze will be present over the fire to contaminate the brightness temperatures, and this effect must be properly examined.

Bright Soils

The brightest surfaces in visible imagery are typically snow or desert sand. In the near infrared, dense vegetation is very bright. But in the SWIR and MWIR, soils are often the brightest surfaces, and in fact soils combined with erratic vegetation cover, such as in agriculture or savannas, can be bright enough in the MWIR to be mistaken for fires. Fortunately, VIIRS possesses a large amount of spectral information that can be used to filter out occurrences of bright soils or non-burning savannas, and the Surface Type EDR will also be of assistance in this regard. Nevertheless, this effect will need to be quantified as part of the Active Fires error budget.

Sunglint

One would not expect a high frequency of fires over the oceans, where sunglint has an established reputation, but even a river or lake can exhibit enough sunglint to induce errors in a fire detection algorithm. Most fire detection algorithms incorporate a sunglint rejection routine. For VIIRS, this will be straightforward, since the Cloud Mask already contains two separate sunglint tests, and the output of these tests is made available to all downstream EDRs. Active Fires will therefore benefit from a system-level solution that must also satisfy the demanding needs of Ocean Color/Chlorophyll and Sea Surface Temperature users, and sunglint rejection should be quite effective at reducing errors in the detection and measurement of fires. The VIIRS land/sea mask will also be of great use in this endeavor.

Atmospheric Effects

The detection of fires relies primarily on the MWIR and LWIR bands, which unavoidably contain significant water vapor absorption features. CO_2 may also be a significant factor in band M13. As discussed in Section 3.3.2.1, atmospheric correction is a key step in the fire detection logic. It is expected that NCEP water vapor analyses will be of sufficient quality to make this error tolerable, but this will need to be verified. For the SWIR bands, water vapor absorption becomes significantly less important, but aerosol scattering plays an increased role. Once a strategy is established for correcting aerosol effects in the SWIR bands as part of fire temperature/area retrieval, sensitivity studies will be conducted to assess the magnitude of the residual errors.

Surface Heterogeneity

The phrase "background characterization" is often loosely used to describe a pivotal part of any fire detection algorithm, however this is not a trivial exercise, for the same reason that many land-based products carry significant uncertainty: surface heterogeneity. The background around an active fire is often not describable by a single parameter or surface type designation, and this leads to errors, especially in fire temperature and area computation. Surface heterogeneity will cause variability in both emissivity and background temperature, both of which are assumed to be known quantities in the application of (1). These effects will need to be assessed before a complete error budget can be constructed.

Natural Variability of Fires

Lastly, but certainly not the least important, are the variations in fires themselves. As already indicated earlier in this document, there are two general regimes for fires—smoldering and flaming. But the spread of temperatures for either scenario is significant. Flaming fires can range over hundreds of degrees K, and smoldering fires can range from 400 to 800 K. This kind of volatility will inevitably lead to some difficulty in pinning down the actual temperature and area, so that even the seemingly "simple" requirement of 50 K uncertainty in fire temperature becomes challenging. These kinds of errors, as with all other important sources of uncertainty, will be explored in Phase II using MODIS combined with higher-resolution satellite data.

3.5 PRACTICAL CONSIDERATIONS

3.5.1 Numerical Computation Considerations

Paragraph SRDV3.2.1.5.4-1 of the VIIRS SRD states the following:

> *"The scientific SDR and EDR algorithms delivered by the VIIRS contractor shall be convertible into operational code that is compatible with a 20 minute maximum processing time at either the DoD Centrals or DoD field terminals for the conversion of all pertinent RDRs into all required EDRs for the site or terminal, including those based wholly or in part on data from other sensor suites."*

RDR here stands for Raw Data Record. This essentially means that any and all EDRs must be completely processed from VIIRS raw data, including calibration and georeferencing, within 20 minutes from the time the raw data are available. This requirement is a strong reminder that VIIRS is an operational instrument.

The Active Fires product exists primarily as a science requirement, however its operational utility is clear, and the HSS provides an excellent example. The kinds of branching decisions involved in the fire detection algorithm can have a more significant impact on computing time than one might first expect, however it is expected that the VIIRS coding effort will produce code that is efficient enough to be used operationally. A principal task for Phase II or beyond is to ensure that solving the system of equations in (1) does not become unstable or require excessive iterations.

3.5.2 Programming and Procedural Considerations

The VIIRS Active Fires code will be developed in concert with developments from MODIS, and its operational aspects will be patterned as much as possible from the HSS processing architecture. These two heritages should reduce the need for extensive programming and procedural resources for the VIIRS Active Fires product. VIIRS Phase II efforts are largely software-focused, and the methodology for this development work is based on sound and proven principles, as discussed in the VIIRS Algorithm Software Development Plan *[Y6635]*. The present maturity of the VIIRS software is detailed in the VIIRS Algorithm Software Maturity Assessment document *[Y6661]*. The maturity and remaining Phase II tasks for the algorithms themselves is summarized in the VIIRS Algorithm/Data Processing Technical Report *[Y7040]*. The software designs relevant to Active Fires are summarized in the VIIRS Context Level Software Architecture *[Y2469]*, Land Module Level Software Architecture *[Y2474]*, Land Module Level Detailed Design *[Y2483]*, and Active Fires Unit Level Detailed Design *[Y3283]*. These designs will be tested at the system level as described in the most recent versions of the VIIRS Software Integration and Test Plan *[Y3236]*, Algorithm Verification and Validation Plan *[Y3237]*, and System Verification and Validation Plan *[Y3270]*. A summary of the ultimate strategy for operational application of the system of VIIRS algorithms is provided in the VIIRS Operations Concept document *[Y2468]*. The VIIRS Interface Control Document (ICD *[Y2470]*) provides more detail on the specifics of ancillary data requirements for Active Fires and other VIIRS products.

3.5.3 Configuration of Retrievals

The Active Fires Application will be configured in tune with the Land Quality Flag (LQF) output appended to the VIIRS Surface Reflectance IP *[Y2411]*. More detail on the exact nature of this configuration will be provided in Version 5 of this ATBD, but a baseline is suggested in the fire detection logic presented in Section 3.3.2.1.

3.5.4 Quality Assessment and Diagnostics

While the LQF output will be the primary descriptor of the Active Fires Application quality, it will be necessary from time to time to run diagnostics on overall algorithm performance, particularly to track calibration behavior in M13, which will not be calibrated for the high radiance range until post-launch observations of gas flares are available. Recommendations on this strategy will be provided in Version 5 of this ATBD.

3.5.5 Exception Handling

Where the LQF output indicates Active Fires should not be retrieved, the EDR fields will be filled with predefined "missing" values. This will be detailed further in Version 5 of this ATBD.

3.6 ALGORITHM VALIDATION

Validation of the VIIRS Active Fires product will follow the lead of validation for the HSS and for MODIS. For the latter, extensive pre-launch campaigns are already available, including MODIS Airborne Simulator (MAS) scenes such as those from the SCAR campaigns. NASA intensive field programs in South America and Africa are being conducted and will continue into the MODIS era, and EOS test sites are established in part to deal with the investigation of fires. AVHRR and GOES also provide platforms for algorithm testing, and the operational use of the HSS will play into validation activities as well. More detail will be provided in Version 5 of this document.

4.0 ASSUMPTIONS AND LIMITATIONS

4.1 ASSUMPTIONS

The following assumptions are made with respect to the retrievals described in this document:

1) The VIIRS Cloud Mask functions at a high level of accuracy, including the treatment of cirrus and the identification of sunglint

2) The VIIRS reflective bands at 865 nm, 1.24 µm, 1.61 µm, and 2.25 µm will be active at night (this is in fact the case in the system and sensor specifications)

3) Dual gain will be implemented for the 4.05 µm band to decouple Fires from Sea Surface Temperature, since the latter would take precedent in any inter-algorithm trades

4) The saturation values for each of the bands associated with the Active Fires product will be retained at their current levels or increased

4.2 LIMITATIONS

The following limitations apply to the at-launch retrievals of described in this document:

1) Active Fires retrievals in the presence of extreme aerosol loading or smoke will be questionable, and spec performance is not guaranteed in these circumstances.

2) Active Fires retrievals for broken clouds (where the central pixel is considered clear or probably clear) may suffer from MTF effects that drive performance below spec; this has not yet been established either way

3) The maturity of using the SWIR bands is quite low at this writing, and must therefore be considered a source of significant risk with regard to system performance

5.0 REFERENCES

Andreae, M. O., (1991). Biomass burning: its history, use, and distribution and its impact on environmental quality and global climate. In: Global Biomass Burning, p.3-21, *J. S. Levine (Ed.). Cambridge, MA: The MIT Press.*

Dozier, J. (1981). A method for satellite identification of surface temperature fields of subpixel resolution, *Remote Sensing of Environment*, 11, 221-229.

Elvidge, C.D., 1997: *Wildfire detection with meteorological satellite data: results from New Mexico during June of 1996 using GOES, AVHRR, and DMSP-OLS*. Report to NOAA-NESDIS, June 16, 1997.

Flasse, S.P., and P. Ceccato, 1996: A contextual algorithm for AVHRR fire detection. *International Journal of Remote Sensing*, 17, 419-424.

Franca, J-R, J-M Brustet, J. Fontan, J-M Gregoire and J. P. Malinggreau (1993). A Multi-spectral remote sensing of biomass burning in West Africa During 90/91 Dry season, Presented at the XVM-EGS General Assembly, May 1993, Wiesbaden, Germany.

Franca, J. Ricardo De A., J.-M. Brustet, and J. Fontan, 1995: Multispectral remote sensing of biomass burning in West Africa. *Journal of Atmospheric Chemistry*, 22, 81-110.

Giglio, L., and J. D. Kendall (2000). Application of the Dozier retrieval to wildfire characterization: a sensitivity analysis. Submitted to *Remote Sensing of Environment*.

Harris, A.J.L., 1996: Towards automated fire monitoring from space: semi-automated mapping of the January 1994 New South Wales wildfires using AVHRR data. *International Journal of Wildland Fire*, 6, 107-116.

IPO (2000). Visible/Infrared Imager/Radiometer Suite (VIIRS) Sensor Requirements Document (SRD) for National Polar-Orbiting Operational Environmental Satellite System (NPOESS) spacecraft and sensors, Rev. 2b/c. Prepared by Assoc. Directorate for Acquisition, NPOESS Integrated Program Office, Silver Spring, MD.

Justice, C.O., and P. Dowty (1993), *IGBP-DIS satellite fire detection algorithm workshop technical report*, IGBP-DIS Working Paper No. 9, 88 pp., Feb. 1993, NASA/GSFC, Greenbelt, Maryland.

Kaufman, Y., and C. Justice, 1998: *MODIS Fire Products Algorithm Technical Background Document*, Version 2.2, EOS ID #2741.

Kaufman, Y. J., R. G. Kleidman, and M. D. King (1998). SCAR-B fires in the tropics: Properties and remote sensing from EOS-MODIS. *J. Geophys. Res.*, 103, 31955-31968.

Kaufman, Y. J., P. V. Hobbs, V. W. J. H. Kirchoff, P. Artaxo, L. A. Remer, B. N. Holben, M. D. King, D. E. Ward, E. M. Prins, K. M. Longo, L. F. Mattos, C. A. Nobre, J. D. Spinhirne, Q. Ji, A. M. Thompson, J. F. Gleason, S. A. Christopher, and S. –C. Tsay (1998). Smoke, Clouds, and Radiation-Brazil (SCAR-B) experiment. *J. Geophys. Res.*, 103, 31737-31808.

Kaufman, Y. J., A. Setzer, C. Justice, C. J. Tucker, M. C. Pereira and I. Fung. (1990). Remote Sensing of Biomass Burning in the Tropics, In: Fire in the Tropical Biota: Ecosystem Processes and Global challenges, J. G. Goldammer (ed.), Springer-Verlag, Berlin, pp371-399.

Lee, T.F., and P. M. Tag, 1990: Improved detection of hotspots using the AVHRR 3.7 mm channel. *Bulletin of the American Meteorological Society*, 71, 1722-1730.

Levine, J. S.(1991). Global biomass burning: atmospheric, climatic, and biospheric implications, In:. Global Biomass Burning, p.3-21, *J. S. Levine (Ed.). Cambridge, MA: The MIT Press.*

Matson, M., and J. Dozier, 1981: Identification of subresolution high temperature sources using a thermal IR sensor. *Photogrammetric Engineering and Remote Sensing*, 47, 1311-1318.

Matson, M., S.R. Schneider, B. Aldridge, and B. Satchwell, 1984: *Fire detection using the NOAA (National Oceanic and Atmospheric Administration)-series satellites*. NOAA Technical Report NESDIS 7, available from the National Technical Information Service, Springfield, VA 22161.

Matson, M., and B. Holben, 1987: Satellite detection of tropical burning in Brazil. *International Journal of Remote Sensing*, 8, 509-516.

Melinotte, J.M., and O. Arino, 1995: *The Ionia '1-km' Net-Browser experience: quicklook processing and assess statistics*. EOQ, No. 50, Dec. 1995.

Pereira, M. C. and A. W. Setzer (1993). Spectral characteristics of deforestation fires in NOAA/AVHRR images, *Int. J. Remote Sensing*, 14, 583-597.

Planet, W.G. (ed.), (1988). Data extraction and calibration of TIROS-N/NOAA radiometers. NOAA Technical Memorandum NESS 107 – Rev. 1, Oct. 1988. 130 pp.

Prins, E.M., and W.P. Menzel, 1992: Geostationary satellite detection of biomass burning in South America. *International Journal of Remote Sensing*, 13, 2783-2799.

Prins, E.M., and W.P. Menzel, 1996: Monitoring fire activity in the western hemisphere with the new generation of geostationary satellite. *AMS 22nd Conference of Agricultural and Forest Meteorology with Symposium on Fire and Forest Meteorology*, Atlanta, GA, Jan. 28-Feb.2, 1996, p.272-275.

Prins, E.M., and W.P. Menzel, 1996b: Monitoring biomass burning and aerosol loading and transport from a geostationary satellite perspective. *AMS 7th Symposium on Global Change Studes*, Atlanta GA, Jan.28-Feb.2, 1996.

Raytheon Hazard Support System, 1998: *Civil sensor fire, volcanoes, and volcanic ash cloud detection algorithm trade study*, Revision 1, CDRL A004, Technical Report #14.

Robinson, J.M., 1991: Fire from space: global fire evaluation using infrared remote sensing. *International Journal of Remote Sensing*, 12, 3-24.

Saunders and Kriebel, 1988: An improved method for detecting clear-sky and cloud radiance from AVHRR data. *International Journal of Remote Sensing*, 9, 120-150.

Setzer, A.W., and M.C. Pereira, 1991: Operational detection of fires in Brazil with NOAA-AVHRR, presented at the *24th International Symposium on Remote Sensing of Environment*, Rio de Janeiro, Brazil, 27-31 May 1991.

Vickos, J.B., 1991: Télédétection des feux de savanes en Afrique Intertropicale et estimation des emissions de constituents ayant un interêt atmosphérique, (in French), Thèse de doctorate de l'Univ., Paul Sabatier, Toulouse, France.